Proton-Induced Tuning of Electrochemical and Photophysical Properties in Mononuclear and Dinuclear Ruthenium Complexes Containing 2,2′-Bis(benzimidazol-2-yl)-4,4′-bipyridine: Synthesis, Molecular Structure, and Mixed-Valence State and Excited-State Properties†

Masa-aki Haga,*,‡ Md. Meser Ali,‡ Shiro Koseki,‡ Kaori Fujimoto,‡ Akio Yoshimura,§ Koichi Nozaki,§ Takeshi Ohno,§ Kiyohiko Nakajima,|| and Derk J. Stufkens⊥

Department of Chemistry, Faculty of Education, Mie University, 1515 Kamihama, Tsu, Mie 514, Japan, Chemistry Department, Faculty of Science, Osaka University, Machikaneyama, Toyonaka, Osaka 560, Japan, Department of Chemistry, Aichi University of Education, Igaya, Kariya, Aichi 448, Japan, and Anorganisch Chemisch Laboratorium, Universiteit van Amsterdam, J. H. van't Hoff Research Institute, Nieuwe Achtergracht 166, 1018 WV Amsterdam, The Netherlands

Received January 26, 1995⊗

A series of mono- and dinuclear $Ru(bpy)_2$ complexes (bpy = 2,2′-bipyridine) containing 2,2′-bis(benzimidazol-2-yl)-4,4′-bipyridine ($bbbpyH_2$) were prepared. The mononuclear complex $[Ru(bpy)_2(bbbpyH_2)](ClO_4)_2 \cdot CH_3OH \cdot 4H_2O$ was characterized by an X-ray structure determination. Crystal data are as follows: triclinic, space group $P\bar{1}$, $a = 14.443(4)$ Å, $b = 15.392(4)$ Å, $c = 11.675(2)$Å, $\alpha = 101.44(2)°$, $\beta = 107.85(2)°$, $\gamma = 96.36(2)°$, $V = 2380(1)$ Å^3, $Z = 2$. The coordination geometry of the ruthenium(II) ion is approximately octahedral. The dihedral angle between the two pyridyl rings in $bbbpyH_2$ is 9.4(3)°, which is close to coplanar, in the complex. Mono- and dinuclear complexes exhibit broad charge-transfer absorption bands at 420−520 nm and emission at 660−720 nm in CH_3CN solution with lifetimes of 200−800 ns at room temperature. Transient difference absorption spectra and resonance Raman (rR) spectra were used to assign the charge-transfer bands in the 420−520 nm region and to identify the lowest excited states. Both absorption and emission spectra are sensitive to solvent and solution pH. Deprotonation of the dinuclear complex raises the energies of the π^* orbitals of the $bbbpyH_2$ ligand, so that they become closer in energy to the π^* orbitals of bpy. The intervalence band of $[(bpy)_2Ru(bbbpyH_2)Ru(bpy)_2]^{5+}$ is observed at 1200 nm ($\epsilon = 170$ M^{-1} cm^{-1}) in CH_3CN. The value of the electronic coupling matrix element, H_{AB}, was determined as 120 cm^{-1}. Upon deprotonation, the IT band was not observed. It is therefore concluded that a superexchange pathway occurs predominantly via the Ru(II) dπ−$bbbpyH_2$ π^* interaction, since deprotonation decreases the interaction. The role of the intervening fragments in the bridging ligand is discussed from the viewpoint of orbital energies and their orbital mixing with Ru dπ orbitals.

Introduction

Dinuclear and polynuclear Ru complexes bridged by bis bi- and tridentate ligands have received much attention in recent years in connection with the design of molecular electronic devices.[1] An understanding of the basic photoinduced intramolecular electron (or energy) transfer events in these complexes and control of the electron transfer pathway are most crucial for the realization of such molecular electronic or photonic devices. Recent studies have revealed that intramolecular electron transfer events can be governed by several factors, including the donor−acceptor electronic coupling, the free-energy change of the reaction, and the polarity of the solvent.[2] The interaction between donor and acceptor in polynuclear Ru complexes is strongly dependent on the bridging ligand. Thus, the design of the bridging ligand is one of the key steps in realizing molecular electronic devices based on polynuclear Ru complexes. Various *N*-heterocyclic fragments such as pyridine, pyrazine, and pyrimidine have been used to construct bridging ligands.[2g,3] For example, 4,4′-bipyridine, 2,3-bis(2-pyridyl)-pyrazine (dpp), and 2,2′-bipyrimidine each can connect two metal ions, mediating metal−metal electronic interaction through their π-system. For the purpose of designing a new bis bidentate bridging ligand, the selection of the intervening and terminal coordinating fragments is important. The π-donor−π-acceptor properties of the bridging ligand and/or the metal−metal distance can be controlled by choosing the appropriate combination of fragments shown in Scheme 1.[2g,3b] Pyridine-, pyrazine-, and pyrimidine-containing ligands have relatively low-lying π^*-orbitals, and therefore they act as good acceptors. In contrast, the imidazole-containing ligands such as bis(imidazole) are poorer π-acceptors and better π-donors.

One of the advantages of using imidazole-containing ligands is the ability to control orbital energies by proton transfer. As part of our study of proton-induced tuning of chemical properties

† A preliminary version of this paper was presented at the *10th International Symposium on the Photochemistry and Photophysics of Coordination Compounds*, July 27, 1993, Abstract O-10.

‡ Mie University.

§ Osaka University.

|| Aichi University of Education.

⊥ University of Amsterdam.

⊗ Abstract published in *Advance ACS Abstracts,* May 1, 1996.

(1) (a) Balzani, V.; Moggi, L.; Scandola, F. *Supramolecular Photochemistry*; Balzani, V., Ed.; Reidel: Dordrecht, The Netherlands, 1987, p1. (b) Balzani, V.; Scandola, F. *Supramolecular Photochemistry*; Ellis Horwood: Chichester, 1991. (c) Woitellier, S.; Launay, J. P.; Spangler, C. W. *Inorg. Chem.* **1989**, *28*, 758. (d) Launay, J. P. *Molecular Electronic Devices II*; Carter, F. L., Ed.; Marcel Dekker: New York, 1987; p 39. (e) Hopfield, J. J.; Onuchic, J. N.; Beratan, D. N. *Science* **1988**, *241*, 817. (f) Kim, Y.; Lieber, C. M. *Inorg. Chem.* **1989**, *28*, 3990. (g) Kavarnos, G. J. *Fundamentals of Photoinduced Electron Transfer*; VCH Publishers: New York, 1993; p 185. (h) Collin, J.-P.; Harriman, A.; Heitz, V.; Odobel, F.; Sauvage, J.-P. *J. Am. Chem. Soc.* **1994**, *116*, 5679. (i) Constable, E. C.; Thompson, A. M. W. C. *J. Chem. Soc., Dalton Trans.* **1992**, 3467. (j) Whittle, B.; Everest, N. S.; Howard, C.; Ward, M. D. *Inorg. Chem.* **1995**, *34*, 2025.

S0020-1669(95)00083-8 CCC: $12.00

Scheme 1

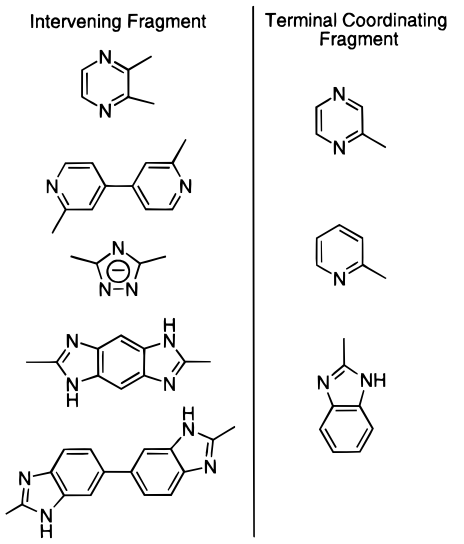

in dinuclear and polynuclear complexes, we have reported earlier[4] the proton-induced switching of metal−metal interactions in dinuclear Ru complexes bridged by 2,2′-bis(2-pyridyl)-bibenzimidazole ($bpbimH_2$). Deprotonation of the intervening benzimidazole moieties appears to induce a large energy perturbation in the dinuclear complex. In the present study, we have extended our investigation to the new bridging ligand system, 2,2′-bis(benzimidazol-2-yl)-4,4′-bipyridine ($4,4'\text{-}bbbpyH_2$),

Scheme 2. Bridging Ligands and Their Abbreviations. The Deprotonated Forms Are Not Shown Here but Abbreviated as 4,4′- or 2,2′-bbbpy and bpbim

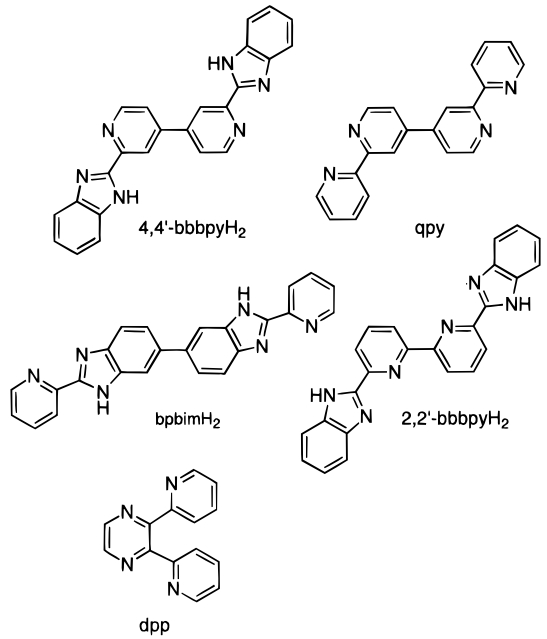

which is one of the structural isomers of $bpbimH_2$ or 6,6′-bis-(benzimidazol-2-yl)-2,2′-bipyridine ($2,2'\text{-}bbbpyH_2$)[5] (Scheme 2). In this $bbbpyH_2$ ligand, the intervening component is a 4,4′-bipyridine, while the $bpbimH_2$ ligand contains the bis(benzimidazole) fragment. Quite recently, the corresponding dinuclear Ru complex containing 2,2′:4′,4″:2″,2‴-quaterpyridine (qpy), also possessing a 4,4′-bipyridine intervening component, as a bridging ligand, has been shown to emit at 685 nm with a surprisingly long lifetime.[6] A comparative study of these 4,4′-bipyridine-based bridging ligands, $4,4'\text{-}bbbpyH_2$ and qpy, with the bis(benzimidazole)-based ligand makes it possible to understand the influence of the bridging ligand, particularly of the intervening part, on the excited-state properties and metal−metal interactions. We describe here the synthesis, molecular structure, and excited-state properties of Ru complexes containing $bbbpyH_2$.

Experimental Section

Materials. 4,4′-Bipyridine (Nacalai) and ruthenium trichloride trihydrate (Engelhardt) were used without further purification. Acetonitrile was purified twice by distillation over P_2O_5. Tetra-*n*-butylammonium tetrafluoroborate (TBAB, Nacalai) was recrystallized from ethanol−water (4:1 v/v) and dried *in vacuo*. All other supplied chemicals were of standard reagent grade quality.

Synthesis. The compounds 2,2′-dicyano-4,4′-bipyridine,[7] 4,4′-bis-(trifluoromethyl)-2,2′-bipyridine (btfmb),[8] $Ru(bpy)_2Cl_2\cdot 2H_2O$,[9] $Ru(btfmb)_2Cl_2\cdot 2H_2O$,[8] $Os(bpy)_2Cl_2\cdot 2H_2O$,[9] and $Ru(bpy\text{-}d_8)_2Cl_2\cdot 2H_2O$[10] were synthesized according to literature methods. ***Caution!*** *Perchlorate salts are potentially explosive. Although no detonation tendencies have been*

(2) (a) Ohno, T. *Prog. React. Kinet.* **1988**, *14*, 219. (b) Scandola, F.; Bignozzi, C. A.; Chiorboli, C.; Indelli, M. T.; Rampi, M. A. *Coord. Chem. Rev.* **1990**, *97*, 299−312. (c) Petersen, J. D. *Supramolecular Photochemistry*; Balzani, V., Ed.; Reidel: Dordrecht, The Netherlands, 1987; p 135. (d) Lehn, J.-M. *Ibid*. p 29. (e) Bignozzi, C. A.; Roffia, S.; Chiorboli, C.; Davila, J.; Indelli, M. T.; Scandola, F. *Inorg. Chem.* **1989**, *28*, 4350. (f) Rillema, D. P.; Callahan, R. W.; Mack, K. B. *Inorg. Chem.* **1982**, *21*, 2589. (g) Ernst, S.; Kaim, W. *Inorg. Chem.* **1989**, *28*, 1520. (h) De Cola, L.; Belser, P.; Ebmeyer, F.; Barigelletti, F.; Vogtle, F.; von Zelewsky, A.; Balzani, V. *Inorg. Chem.* **1990**, *29*, 495. (i) Hage, R.; Dijkhuis, A. H. J.; Haasnoot, J. G.; Prins, R.; Reedijk, J.; Buchana, B. E.; Vos, J. G. *Inorg. Chem.* **1988**, *27*, 2185. (j) Shaw, J. R.; Webb, R. T.; Schmehl, R. H. *J. Am. Chem. Soc.* **1990**, *112*, 1117. (k) Schanze, K. S.; Neyhart, G. A.; Meyer, T. J. *J. Phys. Chem.* **1986**, *90*, 2182. (l) Curtis, J. C.; Bernstein, J. S.; Meyer, T. J. *Inorg. Chem.* **1985**, *24*, 385. (m) Meyer, T. J. *Prog. Inorg. Chem.* **1983**, *30*, 389. (n) Balzani, V.; Scandola, F. *Photoinduced Electron Transfer, Part D*; Fox, M. A., Chanon, M., Eds.; Elsevier: New York, 1988; p 148. (o) Murphy, W. R.; Brewer, K. J.; Gettliffe, G.; Petersen, J. D. *Inorg. Chem.* **1989**, *28*, 81. (p) Rillema, D. P.; Sahai, R.; Matthews, P.; Edwards, A. K.; Shaver, R. J.; Morgan, L. *Inorg. Chem.* **1990**, *29*, 167. (q) Fuchs, Y.; Lofters, S.; Dieter, T.; Shi, W.; Morgan, R.; Strekas, T. C.; Gafney, H. D.; Baker, A. D. *J. Am. Chem. Soc.* **1987**, *109*, 2691. (r) Hunziger, M.; Ludi, A. *J. Am. Chem. Soc.* **1977**, *99*, 7370. (s) Kalyanasundaram, K.; Nazeeruddin, M. K. *Inorg. Chem.* **1990**, *29*, 1888. (t) Yonemoto, E. H.; Saupe, G. B.; Schmehl, R. H.; Hubig, S. M.; Riley, R. L.; Iverson, B. L.; Mallouk, T. E. *J. Am. Chem. Soc.* **1994**, *116*, 4786. (u) Strouse, G. F.; Schoonover, J. R.; Duesing, R.; Meyer, T. J. *Inorg. Chem.* **1995**, *34*, 2725. (v) Molnar, S. M.; Nallas, G.; Bridgewater, J. S.; Brewer, K. J. *J. Am. Chem. Soc.* **1994**, *116*, 5206.

(3) (a) Constable, E. C.; Steel, P. J. *Coord. Chem. Rev.* **1989**, *93*, 205. (b) Kaim, W.; Kohlmann, S. *Inorg. Chem.* **1990**, *29*, 1898.

(4) (a) Haga, M.; Matsumura-Inoue, T.; Yamabe, S. *Inorg. Chem.* **1987**, *26*, 4148. (b) Ohno, T.; Nozaki, K.; Haga, M. *Inorg. Chem.* **1992**, *31*, 548−555. (c) Ohno, T.; Nozaki, K.; Ikeda, N.; Haga, M. *Electron Transfer in Inorganic, Organic and Biological Systems*; Advances in Chemistry Series 228; American Chemical Society: Washington, DC, 1991; p 215. (d) Haga, M.; Ano, T.; Kano, K.; Yamabe, S. *Inorg. Chem.* **1991**, *30*, 3843−3849. (e) Ohno, T.; Nozaki, K.; Haga, M. *Inorg. Chem.* **1992**, *31*, 4256−4261. (f) Nozaki, K.; Ohno, T.; Haga, M. *J. Phys. Chem.* **1992**, *96*, 10880−10888. (g) Haga, M.; Ano, T.; Ishizaki, T.; Kano, K.; Nozaki, K.; Ohno, T. *J. Chem. Soc., Dalton. Trans.* **1994**, 263−272. (h) Haga, M.; Ali, Md. M.; Maegawa, H.; Nozaki, K.; Yoshimura, A.; Ohno, T. *Coord. Chem. Rev.* **1994**, *132*, 99.

(5) (a) Haga, M.; Hiratsuka, K.; Kato, M.; Kurosaki, H.; Goto, M.; Arakawa, R.; Yano, S. *Chem. Lett.* **1995**, 1143. (b) Haga, M.; Mizushima, K.; Murata, I. Work in progress. To simplify the expression, the abbreviation $bbbpyH_2$ stands for $4,4'\text{-}bbbpyH_2$ in this paper.

(6) Downward, A. J.; Honey, G. E.; Philips, L. F.; Steel, P. J. *Inorg. Chem.* **1991**, *30*, 2259.

(7) Fielden, R.; Summers, L. A. *Experoentia* **1974**, *30*, 843.

(8) Furue, M.; Maruyama, K.; Ogumi, T.; Naiki, M.; Kamachi, M. *Inorg. Chem.* **1992**, *31*, 3792.

(9) Lay, P. A.; Sargeson, A.; Taube, H. *Inorg. Synth.* **1986**, *24*, 291.

(10) Chirayil, S.; Thummel, R. P. *Inorg. Chem.* **1989**, *28*, 813.

observed, caution is advised and handling of only small quantities is recommended.

Synthesis of the Bridging Ligand 2,2′-Bis(benzimidazol-2-yl)-4,4′-bipyridine (bbbpyH$_2$). A mixture of 2,2′-dicyano-4,4′-bipyridine (4.95 g, 24 mM) and *o*-phenylenediamine (5.20 g, 48 mM) in polyphosphoric acid was heated at 180 °C for 14 h. The reaction mixture was then cooled to room temperature and poured into water (600 mL). The solution was neutralized with a 28% NH_3 solution. A greenish precipitate was obtained and washed with methanol several times. Finally, the greenish precipitate was dissolved in methanol (700 mL) by dropwise addition of concentrated HCl. After filtration, reprecipitation was achieved by dropwise addition of a concentrated NH_3 (28%) solution until the solution was neutralized. The precipitate was collected and dried *in vacuo*. Yield: 4.80 g (50%). Mp: >290 °C. Mass spectrum: $m/z = 398$ (M^+); M = $C_{24}H_{16}N_6$. Anal. Calcd for $C_{24}H_{16}N_6 \cdot 0.5H_2O$: C, 72.46; H, 4.27; N, 21.11. Found: C, 72.89; H, 4.27; N, 20.63. ^{1}H NMR (DMSO-d_6): δ 7.22(t, 2H, H(β)), 7.25(t, 2H, H(γ)), 7.55(d, 2H, H(δ)), 7.75(d, 2H, H(α)), 8.08(d, 2H, H(5)), 8.75(s, 2H, H(3)), 8.90(d, 2H, H(6)), and 13.23 (br, 2H, N−H).

Synthesis of the Mononuclear Complex [Ru(bpy)$_2$(bbbpyH$_2$)](ClO$_4$)$_2$·4H$_2$O. 2,2′-Bis(benzimidazol-2-yl)-4,4′-bipyridine (0.18 g, 0.45 mM) was suspended in ethylene glycol and heated for 1 h. Ru(bpy)$_2$Cl$_2$·2H$_2$O (0.21 g, 0.40 mM) was added to the resulting suspension, and the mixture was further heated for 5 h. During this period, the color of the solution changed to red. The resulting solution was cooled to room temperature, and 30 mL of water was added to the solution. Excess free ligand was precipitated from the solution and removed by filtration. A solution of $NaClO_4$ (5 g in 200 mL of H_2O) was added dropwise until precipitation was complete. The precipitate was collected, dried, and dissolved in a minimum quantity of CH_3CN, and the solution was chromatographed on a SP-Sephadex C-25 column with CH_3CN−buffer (1:1 v/v). Adjusting the eluted solution to pH 5.5 led to the elution of a yellow band. The eluate was collected and evaporated to half of its volume. Again, saturated $NaClO_4$ solution was added dropwise to the concentrated eluate, resulting in the formation of a yellow precipitate. The precipitate which formed was collected by filtration. Yield: 0.23 g (50%). Anal. Calcd for $RuC_{44}H_{32}N_{10}Cl_2O_8 \cdot 4H_2O$: C, 49.26; H, 3.76; N, 13.06. Found: C, 48.87; H, 3.65; N, 13.01. Single crystals suitable for X-ray structure analysis were grown from acetone−methanol (4:1) at room temperature.

Synthesis of the Protonated Dinuclear Complex [(bpy)$_2$Ru(bbbpyH$_2$)Ru(bpy)$_2$](ClO$_4$)$_4$·4H$_2$O. A solution of Ru(bpy)$_2$Cl$_2$·2H$_2$O (0.31 g, 0.60 mM) in ethylene glycol was heated for 30 min. Solid bbbpyH$_2$ (0.12 g, 0.30 mM) was added to the reddish-violet solution, and the resulting mixture was refluxed for about 7 h, during which time the solution turned dark red. The solution was cooled to room temperature, and 30 mL of H_2O was added. After filtration, a saturated solution of $NaClO_4$ (5 mL) was added dropwise to the filtrate to complete precipitation. The precipitate was collected by vacuum filtration and dried. The precipitate was dissolved in a minimum amount of acetonitrile, loaded on a SP-Sephadex C-25 column, and eluted with CH_3CN−buffer (1:1 v/v). The desired dinuclear complex was eluted as a second fraction by raising the solution pH to 7. The eluate was concentrated to half of the volume, and addition of saturated $NaClO_4$ solution effected the precipitation of the desired complex, which was collected and recrystallized from acetonitrile−methanol (1:4). Yield: 0.31 g (60%). Anal. Calcd for $Ru_2C_{64}H_{48}N_{14}Cl_4O_{16} \cdot 4H_2O$: C, 45.62; H, 3.35; N, 11.64. Found: C, 45.63; H, 3.50; N, 11.38.

[(bpy-d_8)$_2$Ru(bbbpyH$_2$)Ru(bpy-d_8)$_2$](ClO$_4$)$_4$·H$_2$O. Ru(bpy-d_8)$_2$Cl$_2$·2H$_2$O (0.23 g, 0.42 mM) was suspended in 15 mL of glycerol at 100 °C, and the suspension was stirred under nitrogen for 1 h. Then, solid bbbpyH$_2$ (0.085 g, 0.21 mM) was added, and heating was continued for 10 h. The reddish-brown solution was cooled to room temperature, and 30 mL of water was added. The solution was filtered to remove insoluble impurities, and a saturated $NaClO_4$ aqueous solution was added to the filtrate until complete precipitation occurred. The precipitate was collected and purified by column chromatography on a SP-Sephadex C-25 resin with CH_3CN−buffer (1:1 v/v) by adjusting the solution pH to 7.0 as a second band. Yield: 0.21 g (59%). Anal. Cacld for $Ru_2C_{64}H_{16}D_{32}N_{14}Cl_4O_{16} \cdot H_2O$: C, 46.72; H, 3.17; N, 11.87. Found: C, 46.72; H, 2.94; N,11.91. ^{1}H NMR (DMSO-d_6): δ 5.72 (d, 2H, H(α)), 7.10 (t, 2H, H(β)), 7.45 (t, 2H, H(γ)), 7.86 (d, 4H, H(5) and H(6)), 8.00 (d, 2H, H(δ)), 9.01 (s, 2H, H(3)), and 14.88 (br, 2H, N−H).

[(btfmb)$_2$Ru(bbbpyH$_2$)Ru(btfmb)$_2$](ClO$_4$)$_4$·4H$_2$O. Ru(btfmb)$_2$Cl$_2$·2H$_2$O (0.19 g, 0.24 mM) and bbbpyH$_2$ (0.05 g, 0.12 mM) in ethylene glycol were heated for 8 h, during which period the solution became dark red. The solution was cooled to room temperature and filtered. A red precipitate was obtained upon dropwise addition of a saturated $NaClO_4$ aqueous solution to the filtrate. The precipitate was loaded on a SP-Sephadex C-25 column and eluted with CH_3CN−buffer (1:1 v/v), adjusting the solution pH to 7.0. Yield: 0.18 g (67%). Anal. Calcd for $Ru_2C_{72}H_{40}N_{14}F_{24}Cl_4O_{16} \cdot 4H_2O$: C, 38.79; H, 2.17; N, 8.80. Found: C, 38.69; H, 2.77; N, 8.88.

Synthesis of the Deprotonated Dinuclear Complex [(bpy)$_2$Ru(bbbpy)Ru(bpy)$_2$](ClO$_4$)$_2$·7H$_2$O. A solution of [(bpy)$_2$Ru(bbbpyH$_2$)Ru(bpy)$_2$](ClO$_4$)$_4$·4H$_2$O (0.15 g, 0.086 mM) in methanol was added to a sodium methoxide solution which was made *in situ* by dissolving sodium metal (0.01 g, 0.43 mM) in methanol (10 mL). The color of the solution changed from red to dark red. The solution was heated while stirring for 30 min and then cooled to 0−5 °C in a refrigerator. A reddish-brown microcrystalline solid was collected by filtration. Yield: 0.09 g (67%). Anal. Calcd for $Ru_2C_{64}H_{46}N_{14}Cl_4O_{16} \cdot 7H_2O$: C, 49.97; H, 3.93; N,12.75. Found: C, 49.75; H, 3.83; N,12.61.

[(bpy-d_8)$_2$Ru(bbbpy)Ru(bpy-d_8)$_2$](ClO$_4$)$_2$·H$_2$O. This complex was synthesized in a similar manner to [(bpy)$_2$Ru(bbbpy)Ru(bpy)$_2$](ClO$_4$)$_2$·7H$_2$O, except that [(bpy-d_8)$_2$Ru(bbbpyH$_2$)Ru(bpy-d_8)$_2$](ClO$_4$)$_4$ was used instead of [(bpy)$_2$Ru(bbbpyH$_2$)Ru(bpy)$_2$](ClO$_4$)$_4$·4H$_2$O**.** A reddish-brown microcrystalline solid was obtained. Yield: 67%. ^{1}H NMR (DMSO-d_6): δ 5.49 (d, 2H, H(α)), 6.65 (t, 2H, H(β)), 6.95 (t, 2H, H(γ)), 7.57 (d, 2H, H(6)), 7.66 (d, 2H, H(5)), 7.80 (d, 2H, H(δ)), and 8.75 (s, 2H, H(3)).

Physical Measurements. Electronic absorption spectra were obtained on a Hitachi U-3210 spectrophotometer from 200 to 850 nm and a Hitachi 3400 spectrophotometer from 800 to 2500 nm. NMR spectra were measured with a 270 MHz JEOL spectrometer.

Electrochemical measurements were made at 20 °C with a BAS 100 B/W electrochemical workstation. The working electrode was a glassy-carbon or platinum disk electrode and the auxiliary electrode was a platinum wire. The reference electrode was Ag/AgNO$_3$ (0.01 M in 0.1 M TBAB CH_3CN), abbreviated as Ag/Ag$^+$. The $E_{1/2}$ value for the ferrocenium/ferrocene (Fc$^+$/Fc) couple is +0.09 V vs Ag/Ag$^+$. Spectroelectrochemistry was performed by using a platinum minigrid (80 mesh) working electrode in a thin-layer cell (optical path length 0.05 cm). The cell was placed into the spectrophotometer, and the absorption change was monitored during the electrolysis. Flow electrolysis was performed with the same flow-through cell as reported previously.[4b] pH measurements were made with a TOA Model HM-20E pH meter standardized with buffers of pH 4.01 and 6.89. A 50% acetonitrile−buffer mixture was employed because of the limited solubility of the present complexes in pure aqueous solution, particularly at higher pH. The readings of the pH meter in this mixture are referred to as "apparent" pH unless otherwise stated. Spectrophotometric titrations were performed in an acetonitrile−buffer (1:1 v/v) solution, as described previously.[4d] Buffer systems and pH ranges employed were as follows: $HClO_4$−$NaClO_4$, pH 0−2; Robinson−Britton buffer, pH 2−11.

A Hitachi spectrofluorimeter, Model MPF-2A, was used to measure emission spectra at room temperature. Emission lifetimes were measured by means of the single-photon-counting method on a Horiba NASE-550 nanosecond fluorimeter system. The sample was excited by 500 nm pulses from a hydrogen gas lamp through a Nikon G50 monochromator. Transient absorption spectra were obtained after exposure of the solution to the second harmonic pulse of a Q-switched Nd^{3+}−YAG laser by a procedure described elsewhere.[11]

Resonance Raman spectra were recorded for the complexes in a KNO_3 disk by using a spinning cell and a Dilor XY spectrophotometer. The samples were excited by an SP Model 2016 argon ion laser and a Coherent CR 590 dye laser with Coumarin as the dye. Excitation took

(11) Ohno, T.; Yoshimura, A.; Mataga, N. *J. Phys. Chem.* **1990**, *94*, 4871−4876.

Table 1. Crystallographic Data

complex	$[Ru(bpy)_2(bbbpyH_2)](ClO_4)_2 \cdot CH_3OH \cdot 4H_2O$
formula	$C_{45}H_{44}N_{10}Cl_2O_{13}Ru$
formula weight	1104.9
crystal system	triclinic
space group	$P\bar{1}$
a/Å	14.443(4)
b/Å	15.392(4)
c/Å	11.675(2)
α/°	101.44(2)
β/°	107.85(2)
γ/°	96.36(2)
Z	2
V/Å^3	2380(1)
d_{calcd}/g cm^{-3}	1.54
d_{obsd}/g cm^{-3}	1.55
λ/Å	0.71073 (Mo Kα)
μ(Mo Kα)/cm^{-1}	5.07
T/°C	ambient temp
monochrometer	graphite
crystal color	orange
crystal habit	prismatic
crystal size/mm^3	0.2 × 0.3 × 0.5
scan type	$\theta-2\theta$
$2\theta_{max}$/deg	55
reflcns measd	$+h, \pm k, \pm l$
no. of reflcns measd	9902
no. of reflcns obsd $[\|F_o\| > 3\sigma(\|F_o\|)]$	5524
R^a	0.0756
$R_w{}^b$	0.0690
weighting scheme	$w = [\sigma_{count}{}^2 + (0.020\|F_o\|)^2]^{-1}$

[a] $R = \sum||F_o| - |F_c||/\sum|F_o|$. [b] $R_w = [\sum w(|F_o| - |F_c|)^2/\sum w|F_o|^2]^{1/2}$. The atom scattering factors were taken from *International Tables for X-ray Crystallography*; Kynoch Press: Birmingham, England, 1974; Vol. 4.

place at 457.9, 488, 514.5, 538, and 546 nm. The resonance Raman wavenumbers were calibrated by using the1051 cm^{-1} band of KNO_3 as a standard.

The geometrical structures of the bridging ligand $bbbpyH_2$ and its deprotonated form, bbbpy, were optimized by using an STO-3G basis set[12] within the Hartree−Fock approximation (HF/STO-3G). The HF/3-21G method[13] was employed to obtain more reliable electronic structures at the HF/STO-3G optimized geometries. All calculations were performed by using the quantum chemistry program code GAMESS.[14]

X-ray Crystal Structure Determination. An orange prismatic crystal was sealed on a glass fiber and mounted on a Rigaku AFC-5R diffractometer. Intensity data were collected at ambient temperature using graphite monochromatized Mo Kα radiation (λ = 0.71073 Å). Crystal data and other numerical details of the structure determination and refinement are given in Table 1. Unit cell parameters and the orientation matrix were determined from 25 reflections in the range $20° < 2\theta < 25°$. No significant variation in intensities was observed for three standard reflections during data collection. Data were corrected for Lorentz and polarization effects. The calculations were carried out using a HITAC M-680H computer at the Computer Center of the Institute for Molecular Science. The location of the ruthenium atom was determined by direct methods using SHELXS-86,[15] and the other non-hydrogen atoms were found by the usual Fourier methods using the Universal Crystallographic Computation Program System UNICS III.[16] All non-hydrogen atoms were anisotropically refined. The atomic parameters of non-hydrogen atoms and selected bond lengths and angles are listed in Tables 2 and 3, respectively. Anisotropic thermal parameters (Table S1), complete tables of bond distances and angles (Table S2), and an ORTEP drawing of the crystal structures (Figure S1) are included as Supporting Information.

Scheme 3

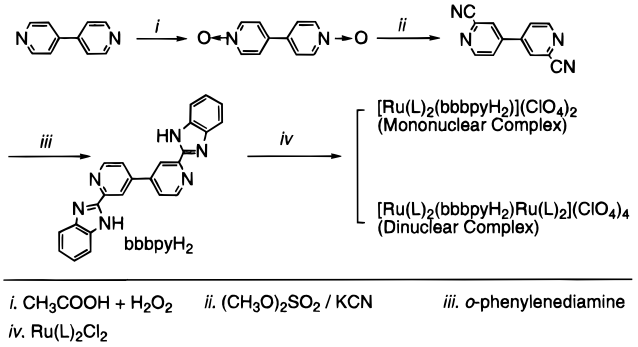

Results and Discussion

Synthesis. The synthetic route to the bridging ligand and its complexes is summarized in Scheme 3. The bridging ligand, $bbbpyH_2$, was synthesized by the condensation reaction of 2,2′-dicyano-4,4′-bipyridine with *o*-phenylenediamine in polyphosphoric acid. The $bbbpyH_2$ ligand is sparingly soluble in common organic solvents. However, the addition of acid such as hydrochloric acid increases the solubility of the ligand in polar organic solvents such as hot methanol. The reaction of $bbbpyH_2$ with $Ru(bpy)_2Cl_2$ in a 1:1 molar ratio gave a mixture of mononuclear and dinuclear complexes. Even when an excess of the ligand was used, the mononuclear complex was always contaminated by the dinuclear complex. Attempts to synthesize only the mononuclear Ru complex have failed so far. To obtain a pure mononuclear complex, the mixture was carefully separated by using SP-Sephadex C-25 cation-exchange chromatography. The structure of the mononuclear complex was confirmed by single crystal X-ray structure analysis described below. The dinuclear complex was obtained by reaction of $Ru(bpy)_2Cl_2$ with the ligand in a 2:1 ratio. Deprotonation was achieved by reaction of sodium methoxide with the mononuclear or dinuclear $bbbpyH_2$ complex in methanol. The deprotonated complexes completely reverted to the corresponding protonated ones by the addition of acid.

NMR Spectra. The ^{1}H NMR spectrum of free $bbbpyH_2$ in DMSO-d_6 shows seven sets of signals in the aromatic region, as illustrated in Figure 1. The signal assignment is rather straightforward if the signal splitting by spin−spin coupling and the comparison of chemical shifts with those of oligopyridines are considered:[17] i.e., proton signals can be assigned to H(6), H(3), H(5), H(α), H(δ), H(γ), and H(β) protons in this order from the low-frequency end (see Figure1 for atom numbering). Figure 1 also shows the ^{1}H chemical shift diagrams of $[(bpy\text{-}d_8)_2Ru(bbbpyH_2)Ru(bpy\text{-}d_8)_2]^{4+}$ and its deprotonated complex in DMSO-d_6. Six proton signal sets are observed for $[(bpy\text{-}d_8)_2Ru(bbbpyH_2)Ru(bpy\text{-}d_8)_2]^{4+}$ in the δ 9.5−5.5 region. This spectral pattern points to a symmetrical two N−N bidentate coordination to Ru ions with respect to the $bbbpyH_2$ bridging

(12) (a) Hehre,W. J.; Stewart, R. F.; Pople, J. A. *J. Chem. Phys.* **1969**, 51. (b) Hehre, W. J.; Ditchfield, R.; Stewart, R. F.; Pople, J. A. *J. Chem. Phys.* **1970**, *52*, 2769.
(13) Binkley, J. S.; Pople, J. A.; Hehre, W. J. *J. Am. Chem. Soc.* **1980**, *102*, 939.
(14) Schmidt, M. W.; Baldridge, K. K.; Boatz, J. A.; Elbert, S. T.; Gordon, M. S.; Jensen, J. H.; Koseki, S.; Matsunaga, N.; Nguyen, K. A.; Su, S.; Windus, T. L.; Dupuis, M.; Montgomery, J. A., Jr. *J. Comput. Chem.* **1993**, *14*, 1347.
(15) Sheldrick, G. M. SHELXS-86, program for crystal structure determination, University of Gottingen, Germany, 1986.
(16) Sakurai, T.; Kobayashi, K. *Rikagaku Kenkyusho Hokoku*, **1979**, *55*, 69.
(17) (a) Xiaoming, X.; Haga, M.; Matsumura-Inoue, T.; Ru, Y.; Addison, A. W.; Kano, K. *J. Chem. Soc., Dalton Trans.* **1993**, 2477. (b) Steel, P. J.; Constable, E. C. *J. Chem. Soc., Dalton Trans.* **1990**, 1389. (c) Haga, M. *Inorg. Chim. Acta* **1983**, *77*, L39−41.

Table 2. Atomic Coordinates ($\times 10^4$) and Equivalent Isotropic Temperature Factors ($Å^2$)

atom	*x*/*a*	*y*/*b*	*z*/*c*	B_{eq}($Å^2$)	atom	*x*/*a*	*y*/*b*	*z*/*c*	B_{eq}($Å^2$)
Ru(1)	2313.8(5)	3013.9(4)	309.8(6)	3.3	C(29)	3758(5)	4649(5)	873(7)	4.5
N(1)	1909(4)	1776(4)	652(5)	3.6	C(30)	4145(6)	4235(5)	1913(7)	4.6
N(2)	3084(4)	2196(3)	−567(5)	3.4	C(31)	5007(7)	4615(6)	2889(9)	6.6
N(3)	2898(4)	4170(4)	−7(6)	4.1	C(32)	5296(7)	4185(7)	3849(9)	7.3
N(4)	3571(4)	3453(4)	1833(5)	3.7	C(33)	4714(7)	3395(6)	3768(8)	6.3
N(5)	1456(4)	3710(4)	1117(5)	4.0	C(34)	3875(6)	3036(5)	2774(7)	4.8
N(6)	1017(4)	2740(4)	−1120(6)	4.4	C(35)	1754(6)	4211(6)	2306(8)	5.9
N(7)	2030(4)	321(4)	380(6)	4.4	C(36)	1120(7)	4651(7)	2769(9)	7.6
N(8)	5759(5)	−945(4)	−2886(6)	4.9	C(37)	163(8)	4586(7)	2069(10)	8.8
N(9)	6446(5)	759(4)	−4365(6)	4.9	C(38)	−161(7)	4076(7)	848(10)	7.5
N(10)	6882(5)	−598(4)	−4283(6)	5.2	C(39)	499(6)	3641(5)	396(8)	4.9
C(1)	1347(5)	1376(5)	1247(7)	4.1	C(40)	246(5)	3071(5)	−872(8)	5.1
C(2)	761(7)	1718(6)	1918(9)	6.1	C(41)	−685(7)	2887(7)	−1727(10)	8.0
C(3)	271(7)	1148(7)	2367(10)	7.7	C(42)	−847(8)	2363(8)	−2917(11)	9.9
C(4)	379(8)	238(7)	2223(10)	7.9	C(43)	−84(7)	2032(6)	−3186(9)	7.9
C(5)	933(7)	−130(5)	1545(9)	6.2	C(44)	831(6)	2237(6)	−2282(8)	5.6
C(6)	1422(5)	459(5)	1085(7)	4.1	C(50)	6600(15)	3294(16)	−2990(18)	22.1
C(7)	2318(5)	1118(4)	162(6)	3.5	O(3A)	6501(11)	2643(9)	−4094(13)	11.7
C(8)	2973(5)	1319(4)	−506(6)	3.2	O(3B)	5914(20)	2621(21)	−3622(28)	20.4
C(9)	3487(5)	709(4)	−973(7)	3.5	Cl(1)	2857(2)	3166(2)	−4386(2)	6.9
C(10)	4128(5)	969(4)	−1540(6)	3.4	Cl(2)	7403(2)	2044(2)	428(3)	8.9
C(11)	4224(5)	1854(5)	−1654(7)	4.2	O(1A)	2095(7)	2938(6)	−3927(9)	13.2
C(12)	3697(6)	2444(5)	−1169(7)	4.2	O(1B)	2791(7)	3976(5)	−4789(8)	11.6
C(13)	4688(5)	322(5)	−2019(6)	3.8	O(1C)	3775(6)	3312(6)	−3454(8)	13.7
C(14)	5240(5)	512(5)	−2761(7)	3.9	O(1D)	2772(8)	2466(5)	−5420(8)	13.1
C(15)	5757(5)	−146(5)	−3157(7)	4.1	O(2A)	7481(11)	1279(6)	783(12)	15.1
C(16)	5216(6)	−1117(5)	−2183(7)	4.8	O(2B)	8141(19)	2693(15)	1604(19)	15.6
C(17)	4689(5)	−514(5)	−1729(7)	4.3	O(2C)	6636(19)	2379(13)	1108(25)	15.7
C(18)	6356(6)	31(5)	−3940(7)	4.6	O(2D)	7731(18)	1716(14)	−763(20)	14.3
C(19)	7082(6)	596(6)	−5041(7)	5.1	O(2E)	7319(15)	2479(15)	−357(20)	12.9
C(20)	7430(7)	1140(6)	−5730(8)	6.3	O(2F)	8493(28)	2036(28)	1092(44)	12.7
C(21)	8078(7)	817(7)	−6274(8)	7.9	O(2G)	6886(22)	1316(21)	5(29)	22.0
C(22)	8381(7)	−17(7)	−6176(9)	8.1	O(2H)	8035(12)	2714(11)	801(17)	10.6
C(23)	8041(7)	−548(7)	−5548(9)	7.1	O(2I)	6463(12)	2158(12)	−101(21)	14.0
C(24)	7374(6)	−239(6)	−4990(7)	5.3	O(31)	738(13)	4229(12)	−4099(14)	21.5
C(25)	2497(6)	4498(5)	−1006(8)	4.9	O(32)	8769(23)	3843(25)	−5815(28)	20.5
C(26)	2921(7)	5295(6)	−1177(9)	6.2	O(33)	7550(21)	3516(15)	4257(32)	19.1
C(27)	3780(7)	5756(5)	−290(9)	6.6	O(34)	9653(23)	3643(31)	4583(32)	25.3
C(28)	4226(6)	5438(5)	756(9)	6.0					

[a] $B_{eq} = 4/3\{\sum_i \sum_j B_{ij} \boldsymbol{a}_i \cdot \boldsymbol{a}_j\}$.

ligand. Protons H(β), H(γ), and H(δ) on the benzimidazole moiety exhibit relatively broad signals due to the N−H proton exchange with residual water in DMSO-d_6. When the spin−spin coupling, the magnetic anisotropy from the bpy ligands, and the chemical shifts of other benzimidazole complexes are considered,[17] the triplet signals at δ 7.10 and 7.45 are assigned to H(β) and H(γ) and the doublet signals at 5.72 and 8.00 to H(α) and H(δ), respectively. Among these benzimidazole protons, the proton H(α) shows a large negative shift upon coordination due to magnetic anisotropy induced by the proximate ring current. The singlet at δ 9.01 can be assigned to H(3) on the pyridine ring. The other H(5) and H(6) pyridine proton signals overlap at δ 7.86. On coordination to two ruthenium ions, the chemical shifts of the H(3), H(γ), and H(δ) are shifted downfield, while the H(5), H(6), H(α), and H(β) show upfield shifts. The deprotonation of $bbbpyH_2$ in the dinuclear complex induces an upfield shift for all proton signals. In particular, H(β) and H(γ) show large upfield shifts. This result indicates that negative charge is accumulated above the carbon atoms attached to H(β) and H(γ) as a result of the deprotonation. This interpretation is supported by the *ab initio* MO calculations of the free $bbbpyH_2$ ligand for the protonated and deprotonated forms: i.e., the MO calculations reveal an increase of electron density on the two carbon-H(β) and -H(γ) moieties after the deprotonation.

X-ray Structure Determination of the Mononuclear Complex. Suitable crystals for X-ray crystallography were obtained by slow evaporation of a mixed methanol−acetone solution of the mononuclear complex $[Ru(bpy)_2(bbbpyH_2)](ClO_4)_2$. This complex contained one methanol and four water molecules as a solvate of the crystallization solvent. An ORTEP drawing of the structure of the cation $[Ru(bpy)_2(bbbpyH_{2)})]^{2+}$ with the atomic numbering scheme is displayed in Figure 2. Table 3 contains selected bond distances and angles. The atom positional and thermal parameters arising from the structure determination, complete tables of bond distances and angles, and an ORTEP drawing of the crystal structures are provided as Supporting Information.

The coordination geometry of the ruthenium(II) ion is approximately octahedral, and the metal is coordinated by two bpy ligands oriented in a *cis* geometry and by a $bbbpyH_2$ ligand. The $Ru-N_{bpy}$ distances (2.025−2.046 Å) and $Ru-N_{bbbpyH2}$ distances (2.081−2.090 Å) are all in the range expected for these types of complexes.[18,19] The bond distances in the $bbbpyH_2$ and bpy ligands are normal. The longer Ru−N(1) and −N(2) distances indicate that the $bbbpyH_2$ ligand acts as a weaker σ-donor relative to the bpy ligand.

(18) Rillema, D. P.; Jones, D. S.; Woods, C.; Levey, H. A. *Inorg. Chem.* **1992**, *31*, 2935.

(19) (a) Templeton, J. L. *J. Am. Chem. Soc.* **1979**, *101*, 4906. (b) Eggleston, D. S.; Goldsby, K. A.; Hodgson, D. J.; Meyer, T. J. *Inorg. Chem.* **1985**, *24*, 4573. (c) Bolger, J. A.; Ferguson, G.; James, J. P.; Long, C.; McArdle, P.; Vos, J. G. *J. Chem. Soc., Dalton Trans.* **1993**, 1577. (d) Rillema, D. P.; Taghdiri, D. G.; Jones, D. S.; Keller, C. D.; Worl, L. A.; Meyer, T. J.; Levy, H. A. *Inorg. Chem.* **1987**, *26*, 578. (e) Fennema, B. D. J. R.; de Graaffi, R. A. G.; Hage, R.; Haasnoot, J. G.; Reedijk, J.; Vos, J. G. *J. Chem. Soc., Dalton Trans.* **1991**, 1043.

Table 3. Selected Bond Lengths (Å) and Bond Angles (deg)

Bond Lengths			
Ru(1)−N(1)	2.081(6)	C(8)−C(9)	1.390(10)
Ru(1)−N(2)	2.090(6)	C(9)−C(10)	1.362(12)
Ru(1)−N(3)	2.034(6)	C(10)−C(11)	1.390(10)
Ru(1)−N(4)	2.046(5)	C(10)−C(13)	1.481(11)
Ru(1)−N(5)	2.045(7)	C(11)−C(12)	1.393(12)
Ru(1)−N(6)	2.025(5)	C(13)−C(14)	1.394(12)
N(1)−C(1)	1.388(11)	C(13)−C(17)	1.394(11)
N(1)−C(7)	1.346(10)	C(14)−C(15)	1.412(11)
N(2)−C(8)	1.360(9)	C(15)−C(18)	1.480(13)
N(2)−C(12)	1.355(11)	C(16)−C(17)	1.389(12)
N(3)−C(25)	1.354(11)	C(19)−C(20)	1.422(14)
N(3)−C(29)	1.362(8)	C(19)−C(24)	1.403(13)
N(4)−C(30)	1.353(9)	C(20)−C(21)	1.368(15)
N(4)−C(34)	1.364(11)	C(21)−C(22)	1.415(16)
N(5)−C(35)	1.358(10)	C(22)−C(23)	1.349(17)
N(5)−C(39)	1.361(9)	C(23)−C(24)	1.392(15)
N(6)−C(40)	1.360(11)	C(25)−C(26)	1.389(13)
N(6)−C(44)	1.350(10)	C(26)−C(27)	1.357(11)
N(7)−C(6)	1.380(12)	C(27)−C(28)	1.404(14)
N(7)−C(7)	1.349(10)	C(28)−C(29)	1.375(12)
N(8)−C(15)	1.330(10)	C(29)−C(30)	1.470(12)
N(8)−C(16)	1.340(13)	C(30)−C(31)	1.377(10)
N(9)−C(18)	1.322(11)	C(31)−C(32)	1.391(15)
N(9)−C(19)	1.395(12)	C(33)−C(34)	1.362(10)
N(10)−C(18)	1.367(11)	C(35)−C(36)	1.373(15)
N(10)−C(24)	1.396(12)	C(36)−C(37)	1.354(14)
C(1)−C(2)	1.397(14)	C(37)−C(38)	1.389(14)
C(1)−C(6)	1.407(10)	C(38)−C(39)	1.395(14)
C(2)−C(3)	1.348(16)	C(39)−C(40)	1.475(11)
C(3)−C(4)	1.409(15)	C(40)−C(41)	1.367(11)
C(4)−C(5)	1.378(16)	C(41)−C(42)	1.396(16)
C(5)−C(6)	1.378(13)	C(42)−C(43)	1.358(17)
C(7)−C(8)	1.443(12)	C(43)−C(44)	1.371(11)

Bond Angles			
N(1)−Ru(1)−N(2)	78.3(2)	N(2)−Ru(1)−N(6)	97.8(2)
N(1)−Ru(1)−N(3)	171.9(3)	N(3)−Ru(1)−N(4)	78.6(2)
N(1)−Ru(1)−N(4)	96.7(2)	N(3)−Ru(1)−N(5)	89.7(3)
N(1)−Ru(1)−N(5)	97.3(3)	N(3)−Ru(1)−N(6)	97.3(2)
N(1)−Ru(1)−N(6)	88.1(2)	N(4)−Ru(1)−N(5)	94.4(2)
N(2)−Ru(1)−N(3)	94.9(3)	N(4)−Ru(1)−N(6)	172.3(2)
N(2)−Ru(1)−N(4)	89.2(2)	N(5)−Ru(1)−N(6)	78.9(2)
N(2)−Ru(1)−N(5)	174.6(2)		

The dihedral angle between both pyridyl rings in the $bbbpyH_2$ ligand is 9.4(3)°, which is close to coplanar, in the complex. No significant intermolecular interactions such as hydrogen bonding or stacking interactions between aromatic rings could be found. Several X-ray structures of the 4,4′-bipyridine complexes have been reported, some of which adopt a coplanar structure.[20]

In order to shed light on the electronic structure of $bbbpyH_2$, *ab initio* molecular orbital calculations were performed. The most interesting feature of the HOMO (71st) and LUMO (72nd) orbitals is the electron density distribution of these two orbitals (Figure 3). In the HOMO, the electron density is concentrated on the benzimidazolyl moieties.

On the other hand, the contour lines of the electron density in the LUMO are concentrated on the central 4,4′-bpy moieties, which indicates that the electron occupation of this orbital has a large quinoid contribution. If $bbbpyH_2$ is behaving as a π-acceptor and Ru(II) as a π-donor, the LUMO of the $bbbpyH_2$ ligand can be significantly occupied. Furthermore, the electronic structures of $bbbpyH_2$ coordinated to F^- and H^+ were calculated as model systems for the coordination of the electron donor and electron acceptor. The result of the *ab initio* MO calculations clearly indicates that coordination of an electron donor such as F^- prefers the coplanar structure, whereas in the case of an electron acceptor such as H^+ the nonplanar structure is adopted. Thus, these *ab initio* MO calculations support the planar structure of the $bbbpyH_2$ ligand when the Ru(II) ion acts as an electron donor. A similar interpretation has been proposed for the dihedral angles of the biphenyl C−C bond in the tetraaminobiphenyl $Ru(bpy)_2$ complex, and the possibility for this complex to act as a molecular switch by this twisting of the biphenyl C−C subunit has then been noted.[21] Recently, conformational changes induced by complexation with a cation or by photoexcitation have been shown to modify the electron transfer properties of these complexes.[22] Similarly, the present mononuclear complex has the potential to undergo a conformational change around the 4,4′-bipyridine C−C bond in response to a perturbation such as the Ru(II) to Ru(III) oxidation.

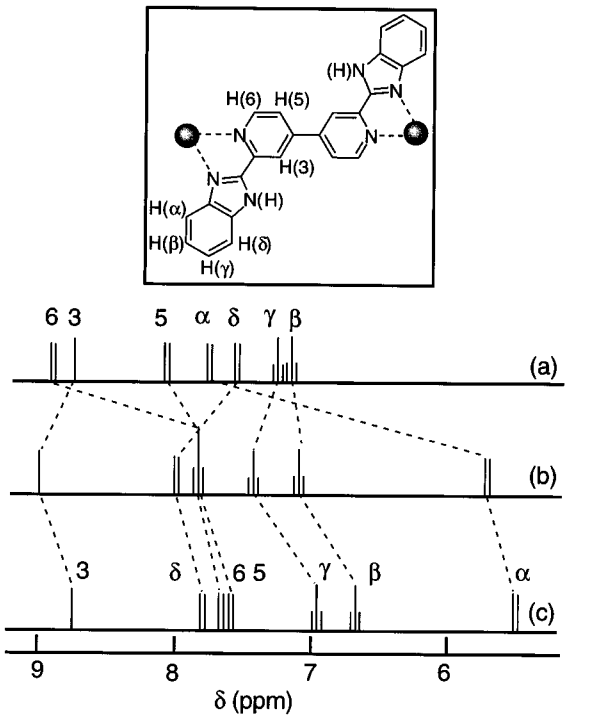

Figure 1. ^1H NMR chemical shift diagram (270 MHz) of (a) the free $bbbpyH_2$ ligand (b) dinuclear $[(bpy\text{-}d_8)_2Ru(bbbpyH_2)Ru(bpy\text{-}d_8)_2]^{4+}$, and (c) its deprotonated complex in DMSO-d_6.

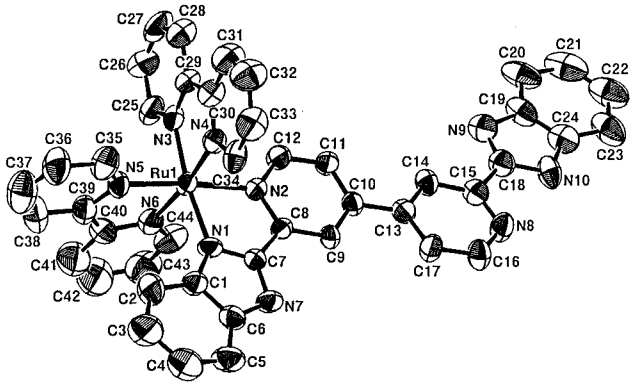

Figure 2. An ORTEP diagram of the structure of the cation $[Ru(bpy)_2(bbbpyH_2)]^{2+}$ with the atomic numbering scheme.

(20) (a) Das,A.; Jeffery, J. C.; Maber, J. P.; McCleverty, J. A.; Schatz, E.; Ward, M. D.; Wollermam, G. *Inorg. Chem.* **1993**, *32*, 2145. (b) Julve, M.; Verdaguer, M.; Faus, J.; Tinti, F.; Moratal, J.; Monge, A.; Gutierrez-Puebla, E. *Inorg. Chem.* **1987**, *26*, 3520.

(21) Metcalfe, R. A.; Dodsworth, E. S.; Lever, A. B. P.; Pietro, W. J.; Stufkens, D. J. *Inorg. Chem.* **1993**, *32*, 3581.

(22) (a) Gourdon, A. *New J. Chem.* **1992**, *16*, 953−957. (b) Chen, P.; Curry, M.; Meyer, T. J. *Inorg. Chem.* **1989**, *28*, 2271−2280.

Table 4. Absorption and Emission Spectral Data of Mononuclear and Dinuclear Ru Complexes with Various Bridging Ligands in CH_3CN

complex	absorption maxima, ϵ [nm (M^{-1} cm^{-1})] bpy($\pi-\pi^*$)	BL($\pi-\pi^*$)	MLCT (d$\pi-\pi^*$)	emission maxima (nm)	lifetime at room temp (ns)
$[Ru(bpy)_2(bbbpyH_2)]^{2+}$	289 (69 100)	328 (36 800)	465 (15 100)	668	880
$[Ru(bpy)_2(bbbpyH)]^{+}$	293 (67 500)	335 (33 500)	476 (11 400)		
$[Ru_2(bpy)_4(bbbpyH_2)]^{4+}$	289 (128 000)	342 (46 000)	460 sh, 498 (31 500)	719	210[e]
$[Ru_2(bpy)_4(bbbpy)]^{2+}$	293 (145 500)	344 (59 300)	486 (43 800)		
$[Ru_2(btfmb)_4(bbbpyH_2)]^{4+}$	298 (129 000)	342 (50 500)	477 (38 400)	672	360
$[Ru_2(btfmb)_4(bbbpy)]^{2+}$	300 (89 800)	342 sh, 345 (35 500)	461 (19 600), 512 sh		
$[Ru(bpy)_2(qpy)]^{2+}$ [a]			455 (120 000)		
$[Ru_2(bpy)_4(qpy)]^{4+}$ [a]	287 (110 000)		471 (22 000)	685	2000
$[Ru(bpy)_2(bpbimH_2)]^{2+}$ [b]	289 (79 900)	346 (37 900)	459 (15 300)	635	480
$[Ru_2(bpy)_4(bpbimH_2)]^{4+}$ [b]	289 (136 000)	355 (53 500)	459 (27 000)	640	560
$[Ru(bpy)_2(dpp)]^{2+}$ [c]	284 (66 600)		468 (11 000)	691	380
$[Ru_2(bpy)_4(dpp)]^{4+}$ [c]	284 (115 000)		526 (24 700)	802	125
$[Ru(bpy)_2(bpt)]^{+}$ [d]			475 (11 300)	678	160
$[Ru_2(bpy)_4(bpt)]^{3+}$ [d]			453 (22 600)	648	100

[a] Reference 5. [b] Reference 4b. [c] Reference 2s. [d] Reference 2c. [e] The lifetimes of the deuteriated complex $[Ru_2(bpy\text{-}d_8)_4(bbbpyH_2)]^{4+}$ are 202 ns in CH_3CN, 233 ns in CD_3CN, 282 ns in CD_3CN with 1 mM DCl, and 109 ns in the CD_3CN/D_2O mixture.

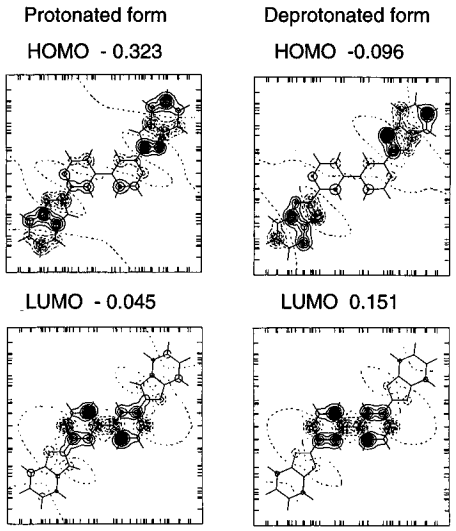

Figure 3. The contour plots for the HOMO (71th) and LUMO (72th) orbitals of the bridging ligand $bbbpyH_2$ for protonated and di-deprotonated forms, obtained by *ab initio* MO calculations. The contour lines show the electron density in the section. Each number represents the orbital energy as a hartree unit.

Absorption Spectra of Protonated Complexes. Absorption spectral data are collected in Table 4. Mononuclear $[Ru(bpy)_2(bbbpyH_2)]^{2+}$ has a d$\pi-\pi^*$(MLCT) absorption maximum at 465 nm in CH_3CN. The $\pi-\pi^*(bbbpyH_2)$ transition appeared at 329 nm. Going from the mononuclear compound to the dinuclear complex $[(bpy)_2Ru(bbbpyH_2)Ru(bpy)_2]^{4+}$, the absorption maxima of both the d$\pi-\pi^*$ and $\pi-\pi^*(bbbpyH_2)$ transitions shift to longer wavelength (Table 4). This result indicates that coordination of the second Ru(II) ion stabilizes the π^*-level of $bbbpyH_2$. The MLCT absorption maximum is slightly lower in energy than those of $[Ru(bpy)_2(bpbimH_2)]^{2+}$ and $[Ru(bpy)_2(bpbimH_2)Ru(bpy)_2]^{4+}$ but higher than those of $[Ru(bpy)_2(dpp)]^{2+}$ and $[(bpy)_2Ru(dpp)Ru(bpy)_2]^{4+}$.[2s] This shows that the donor property of the bridging ligand decreases in the order of $bpbimH_2$ > $bbbpyH_2$ > dpp. In the case of substitution of the peripheral bpy ligands by btfmb, the MLCT band of the dinuclear complex shifts to shorter wavelength. Since btfmb is a weak σ-donor, as a result of the strongly electron-withdrawing substituents and low π^*-orbital energies, the dπ orbitals will also be stabilized. The lowering in energy of both the dπ and peripheral ligand π^*-orbitals is responsible for the change of MLCT band energies.

Emission Spectra. The MLCT emission of $[Ru(bpy)_2(bbbpyH_2)]^{2+}$ is observed at 668 nm in CH_3CN. Addition of perchloric acid leads to quenching of the emission, and the lifetime becomes shorter (25 ns).

$[(bpy)_2Ru(bbbpyH_2)Ru(bpy)_2]^{4+}$ in CH_3CN emits at 719 nm-(uncorrected) with a lifetime of 200 ns. The emission maximum of the dinuclear complex was observed at longer wavelength compared to that of the mononuclear complex. Substitution of the peripheral ligand bpy by btfmb in $[(L)_2Ru(bbbpyH_2)Ru(L)_2]^{4+}$ leads to a blue shift in the emission maximum. Addition of water to the CH_3CN solution of the dinuclear complex $[(bpy)_2Ru(bbbpyH_2)Ru(bpy)_2]^{4+}$ decreases the emission intensity and its lifetime drastically. The hydrogen-bonding interaction of the imino NH moiety of $bbbpyH_2$ is responsible for the change in excited-state properties, in which the N−H moiety acts as a H^+ donor and the water as a H^+ acceptor. This interaction between the imino NH group and the solvent makes the nonradiative decay pathway more efficient due to the lowering of dd state energies. This is supported by the decrease of the oxidation potential under these conditions.

When the peripheral bpy is deuterated in $[(bpy\text{-}d_8)_2Ru(bbbpyH_2)Ru(bpy\text{-}d_8)_2]^{4+}$, no change is observed in the emission maxima and lifetime. However, when deuterated hydrochloric acid was added to the solution, the lifetime became 40% longer. The observed deuterium effect can be explained by the H/D exchange on the imino moiety.

The present $bbbpyH_2$ dinuclear complex exhibits a 10 times shorter excited-state lifetime, compared to the qpy-bridged dinuclear complex (2.0 μs in CH_3CN).[6] Since the intervening 4,4′-bipyridine component is the same for $bbbpyH_2$ and qpy, the change of the excited-state properties will be caused by the difference in the terminal coordinating components benzimidazole and pyridine.

Electrochemistry of Protonated Complexes. Redox potentials of the ruthenium complexes are collected in Table 5. The mononuclear complex $[Ru(bpy)_2(bbbpyH_2)]^{2+}$ reveals a one-electron oxidation process at +0.79 V vs Fc/Fc^+ and three one-electron reduction processes at −1.44, −1.72, and −1.99 V. In the reduction processes, the first reduction was irreversible at a scan rate of 100 mV s^{-1}. However, reversible behavior was observed at scan rates of 1 V s^{-1} or above. The oxidation is a Ru(II/III) process, which can be proven by the disappearance of the MLCT band after the oxidative spectroelectrochemistry at +0.9 V. From the reduction potential of $[Ru(bpy)_3]^{2+}$ in CH_3CN,[23] it is concluded that reduction of the mononuclear

Table 5. Electrochemical Data for Ru Mononuclear and Dinuclear Ru Complexes in CH_3CN at a Platinum Electrode at Room Temperature

	V vs Fc/Fc^+ (ΔE, mV)[b]	
complex	oxidation[a]	reduction[a]
$[Ru(bpy)_2(bbbpyH_2)]^{2+}$	0.79 (65)	−1.44 (irr),[c] −1.72 (100), −1.99 (64)
$[Ru_2(bpy)_4(bbbpyH_2)]^{4+}$	0.80 (65)	−1.32 (62), −1.71 (57), −1.95 (100)
$[Ru_2(bpy)_4(bbbpy)]^{2+}$	0.37 (67)	−1.71 (70), −1.93 (90)
$[Ru_2(btfmb)_4(bbbpyH_2)]^{4+}$	1.08 (69)	−1.30 (61), −1.52 (62), −1.91 (85)
$[Ru_2(btfmb)_4(bbbpy)]^{2+}$	0.59 (68)	−1.36 (72), −1.59 (70), −1.94 (84)
$[Ru(bpy)_2(qpy)]^{2+}$ [d]	0.82	−1.70, −1.89, −2.23
$[Ru_2(bpy)_4(qpy)]^{4+}$ [d]	0.84	−1.48, −1.82, −1.95, −2.02
$[Ru_2(bpy)_4(bpbimH_2)]^{4+}$ [e]	0.77	−1.78, −1.87, −2.14
$[Ru(bpy)_2(dpp)]^{2+}$ [f]	0.92	−1.44, −1.93, −2.12
$[Ru_2(bpy)_4(dpp)]^{4+}$ [f]	1.16, 0.99	−1.05, −1.55, −1.95

[a] The peak-to-peak separation is given in parentheses at a scan rate of 100 mV s^{-1}. [b] Peak-to-peak separation is given in parentheses. [c] Quasireversible wave at a scan rate of 1V s^{-1}. [d] Reference 6. [e] Reference 4b. [f] Reference 2c.

complex occurs first on the $bbbpyH_2$ ligand and then on each bpy ligand (Table 5).

The dinuclear complex $[(bpy)_2Ru(bbbpyH_2)Ru(bpy)_2]^{4+}$ exhibits only one oxidation wave. No difference in the oxidation potential was observed between the mononuclear and the dinuclear complex (Table 5). Coulometry indicates that two electrons are involved in this process. From the separation between the anodic and cathodic peak potential (65 mV),[24] it is concluded that two closely spaced one-electron processes are involved in this oxidation. Upon deprotonation of the dinuclear complex, the oxidation potential shifts to a more negative potential (about 0.4 V) while the peak-to-peak separation in the dinuclear complex does not change.

Coordination of the second $[Ru(bpy)_2]^{2+}$ ion to the remote nitrogen atoms of the mononuclear $[Ru(bpy)_2(bbbpyH_2)]^{2+}$ causes a shift to more positive potential for the reduction processes with respect to the mononuclear complex, particularly for the first reduction process. This potential shift reflects the stabilization of the $bbbpyH_2$ π^*-orbitals in the dinuclear complex, which is consistent with the lower energies of both the $\pi-\pi^*(bbbpyH_2)$ and MLCT transitions of the dinuclear complex. From the combined electrochemical and photophysical data, the redox sites for the dinuclear complex can be assigned to the Ru(II/III) couple for the oxidation and the successive reductions to first the bridging $bbbpyH_2$ and then to the two bpy ligands. A sharp spike due to adsorption onto the electrode was observed in the third reduction wave. The oxidation potential for $[(bpy)_2Ru(BL)Ru(bpy)_2]^{4+}$ increases in the order of BL = $bpbimH_2$ < $bbbpyH_2$ < qpy < dpp, which indicates that the acceptor property of the bridging ligand BL increases in this order.

The introduction of trifluoromethyl groups into the bpy ligand leads to a large positive shift of the Ru(II/III) oxidation potential (Table 5). The dinuclear complex $[(btfmb)_2Ru(bbbpyH_2)Ru(btfmb)_2]^{4+}$ exhibits a two-electron oxidation process at +1.08 V in CH_3CN, which is shifted to a 0.28 V more positive potential than that of the bpy analog. Three reversible one-electron reduction processes for $[(btfmb)_2Ru(bbbpyH_2)Ru(btfmb)_2]^{4+}$ were observed at −1.30, −1.52, and −1.91 V. However, the assignment of the reduction processes is not straightforward since the btfmb ligand has its π^* orbitals at lower energy.[25] Deprotonation of the $bbbpyH_2$ ligand does not affect these reduction potentials. Both btfmb and $bbbpyH_2$ reduction waves may be overlapping.

Resonance Raman (rR) Spectra of Protonated Complexes. To characterize which ligand is involved in the lowest energy MLCT transition in the present mixed-ligand Ru complexes, rR spectra were obtained. Because of the strong emission, rR spectra of $[Ru(bpy)_2(bbbpyH_2)]^{2+}$ could only be obtained with excitation wavelengths of 458−488−496.5 nm. All three rR spectra show the presence of bands belonging to bpy and $bbbpyH_2$. However, the $bbbpyH_2$ bands at 1618, 1451, and 1274 cm^{-1} decrease in intensity with respect to the bpy bands[2q,26] at 1603, 1554, 1487, 1317, 1287, and 1173 cm^{-1} when the exciting wavelength is varied from 496.5 to 458 nm. The intensity ratio of the two bands at 1618 and 1603 cm^{-1} changes from ca. 1:1 with 496.5 nm excitation to 1:3 with excitation at 458 nm. The wavelength dependence of these intensities demonstrates how the MLCT transitions and accordingly the character of the lowest empty ligand orbital varies with the wavelength of excitation.[26] Thus, the MLCT absorption maximum at 460 nm mainly belongs to the Ru to $bbbpyH_2$ MLCT transitions and the high-energy shoulder to Ru−bpy MLCT.

Since the absorption spectrum of the dinuclear complex $[(bpy)_2Ru(bbbpyH_2)Ru(bpy)_2]^{4+}$ in CH_2Cl_2 shows two absorption maxima at ∼490 and ∼460 nm, rR spectra have been obtained with 457.9−488−514.5 and 536 nm excitation. The rR spectrum of $[(bpy)_2Ru(bbbpyH_2)Ru(bpy)_2]^{4+}$ excited at 514.5 nm shows the highest rR intensities for $bbbpyH_2$ bands at 1616, 1267, and 1024 cm^{-1} (Figure 4). Going to shorter wavelength excitation, the relative intensities of these bands decrease with respect to those of bpy. At 488 nm, both the $bbbpyH_2$ and bpy bands have a similar contribution, and the bpy bands further increase upon 457.9 nm excitation. From this wavelength dependence, we can conclude that the first absorption maximum at 490 nm mainly belongs to Ru to $bbbpyH_2$ transitions and the second one at ∼460 nm to Ru to bpy transitions.

Upon substitution of the peripheral bpy ligands by btfmb in $[(bpy)_2Ru(bbbpyH_2)Ru(bpy)_2]^{4+}$, the spectral changes are less clear because unfortunately two of the $bbbpyH_2$ vibrations

(23) (a) Juris, A.; Balzani, V.; Barigelletti, F.; Campagna, S.; Belser, P.; von Zelewsky, A. *Coord. Chem. Rev.* **1988**, *84*, 85. (b) Kalyanasundaram, K. *Photochemistry of Polypyridine and Porphyrin Complexes*; Academic Press: London, 1991.
(24) Richardson, D. E.; Taube, H. *Inorg. Chem.* **1981**, *20*, 1278−1285.
(25) Furue, M.; Maruyama, K.; Oguni, T.; Naiki, M.; Kamachi, M. *Inorg. Chem.* **1992**, *31*, 3792−3795.
(26) (a) Stufkens, D. J.; Snoeck, Th. L.; Lever, A. B. P. *Inorg. Chem.* **1988**, *27*, 953. (b) Caswell, D. S.; Spiro, T. G. *Inorg. Chem.* **1987**, *26*, 18−22. (c) Mabrouk, P. A.; Wrighton, M. S. *Inorg. Chem.* **1986**, *25*, 526−531. (d) Hage, R.; Haasnoot, J. G.; Stufkens, D. J.; Snoeck, Th. L.; Vos, J. G.; Reedijk, J. *Inorg. Chem.* **1989**, *28*, 1413. (e) Mallick, P. K.; Danzer, G. D.; Strommen, D. P.; Kincaid, J. R. *J. Phys. Chem.* **1988**, *92*, 5628. (f) Nazeeruddin, M. K.; Gratzel, M.; Kalyanasundaram, K.; Girling, R. B.; Hester, R. E. *J. Chem. Soc., Dalton Trans.* **1993**, 323−325. (g) Fuchs, Y.; Lofters, S.; Dieter, T.; Shi, W.; Morgan, R.; Strekas, T. C.; Gafney, H. D.; Baker, A. D. *J. Am. Chem. Soc.* **1987**, *109*, 2691.

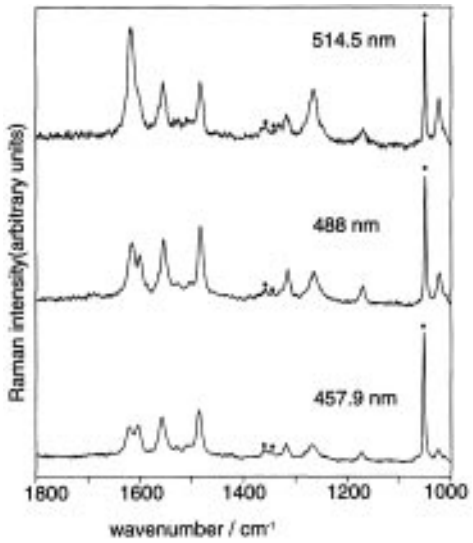

Figure 4. Resonance Raman spectra of the dinuclear complex $[(bpy)_2Ru(bbbpyH_2)Ru(bpy)_2](ClO_4)_4$ in a KNO_3 pellet at room temperature at different excitation wavelengths. Bands marked with an asterisk are NO_3^- bands, used as a standard.

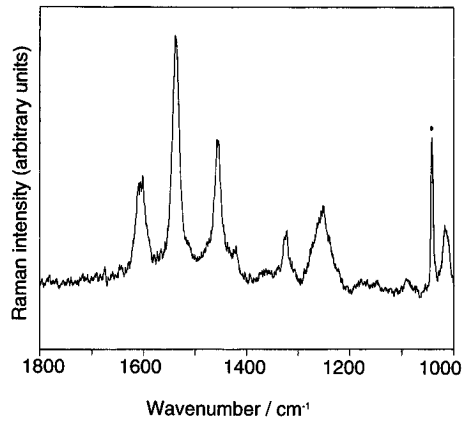

Figure 5. Resonance Raman spectrum of $[(btfmb)_2Ru(bbbpyH_2)Ru(btfmb)_2](ClO_4)_4$ in a KNO_3 pellet at room temperature obtained by excitation at 488 nm. The band marked with an asterisk belongs to NO_3^-.

coincide with btfmb modes at ~1625 and 1270 cm^{-1}. However, dinuclear $[(btfmb)_2Ru(bbbpyH_2)Ru(btfmb)_2]^{4+}$ exhibits the highest rR intensity for the $bbbpyH_2$ bands at 1625, 1268, and 1024 cm^{-1} upon 488 nm excitation (Figure 5). The relative intensities of the btfmb bands were highest in the 457.9 nm excited spectrum. Still, these intensity effects are not very dramatic and the Ru → btfmb and Ru → $bbbpyH_2$ transitions will therefore nearly coincide.

Transient Absorption Spectra of Protonated Complexes. The transient difference absorption (TA) spectrum at ambient temperature, obtained immediately after laser excitation of $[Ru(bpy)_2(bbbpyH_2)]^{2+}$ in 1 mM $HClO_4$ in CH_3CN, is shown in Figure 6a. Under neutral conditions, the same TA spectrum is observed for $[Ru(bpy)_2(bbbpyH_2)]^{2+}$. The TA decayed with the same rate as the phosphorescence monitored at 667 nm. This means that the TA spectrum represents the formation of the lowest excited CT state. The TA spectrum of $[Ru(bpy)_2(bbbpyH_2)]^{2+}$ exhibits a strong bleaching of the $\pi-\pi^*$ transition of $bbbpyH_2$ at 334 nm and of the MLCT band at 462 nm and an absorption enhancement at 310, 380, and 540 nm (Figure 6a), which is clearly different from that of $[Ru(bpy)_3]^{2+}$.[27] By

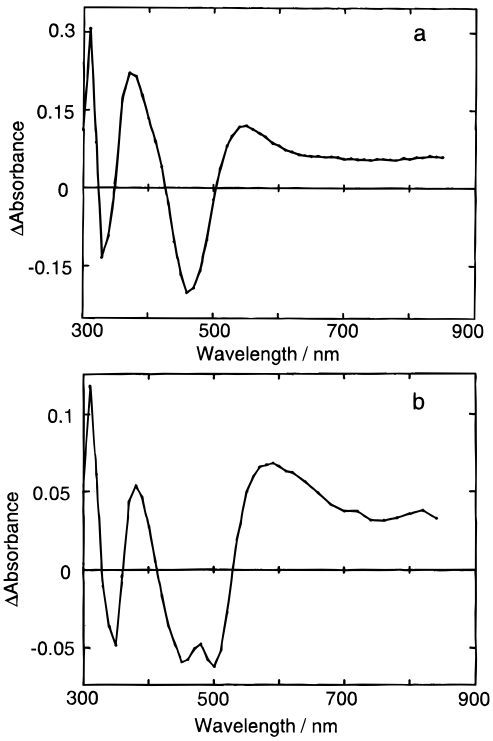

Figure 6. The transient difference absorption (TA) spectra of (a) mononuclear $[Ru(bpy)_2(bbbpyH_2)]^{2+}$ (1.9×10^{-5} M with 1 mM $HClO_4$) and (b) dinuclear $[(bpy)_2Ru(bbbpyH_2)Ru(bpy)_2]^{4+}$ (1.3×10^{-5} M with 1 mM $HClO_4$) in CH_3CN immediately after laser excitation.

comparison with reported spectra of other relevant complexes,[27] the band at 310 nm is assigned to a $\pi-\pi^*$ transition of bpy coordinated to Ru(III), and the bands around 380 and 540 nm are assigned to $\pi-\pi^*$ transitions of reduced $bbbpyH_2^-$. From these results, it is concluded that the lowest excited state of $[Ru(bpy)_2(bbbpyH_2)]^{2+}$ is Ru(II) to $bbbpyH_2$ CT in character, which is consistent with the wavelength dependence of the rR spectra.

The TA spectrum of $[(bpy)_2Ru(bbbpyH_2)Ru(bpy)_2]^{4+}$, shown in Figure 6b, is similar to that of the mononuclear complex, except for a shift to longer wavelength and a splitting of the MLCT band around 480 nm. The observed decay rate for the TA spectra shows the same value as that of phosphorescence at all wavelengths. Therefore, the TA spectrum is ascribed to the formation of an excited MLCT state. The oxidative difference absorption spectrum obtained spectroelectrochemically at +0.9 V indicates a decrease of the MLCT band around 500 nm, the appearance of a LMCT band at 640 nm, and $\pi-\pi^*$ transitions of bpy and $bbbpyH_2$ coordinated to Ru(III) at 310 and 380 nm, respectively. Thus, the TA spectrum of the dinuclear complex reveals that the excited electron resides on the $bbbpyH_2$ bridging ligand. On the contrary, when the peripheral bpy was substituted by btfmb, the TA spectrum of $[(btfmb)_2Ru(bbbpyH_2)Ru(btfmb)_2]^{4+}$ in CH_3CN exhibited an absorption feature similar to that of $[Ru(bpy)_3]^{2+}$ (Figure 7). Since no strong bleaching for the $\pi-\pi^*$ transition of bbbpy at 342 nm is observed and a strong band belonging to $btfmb^-$ shows up at 370 nm, the lowest excited state has Ru → btfmb MLCT character.

Proton-Induced Tuning of the Chemical Properties: Absorption Spectra. The absorption spectra of all complexes in CH_3CN−buffer strongly depend on the solution pH. As the pH of a solution of $[Ru(bpy)_2(bbbpyH_2)]^{2+}$ in CH_3CN−buffer is raised, two stepwise spectral changes are observed at $1 < pH < 10$. From pH 1 to 5.2, the intensity of the valley at 385

(27) Ohno, T.; Yoshimura, A.; Prasad, D. R.; Hoffman, M. Z. *J. Phys. Chem.* **1991**, *95*, 4723−4727.

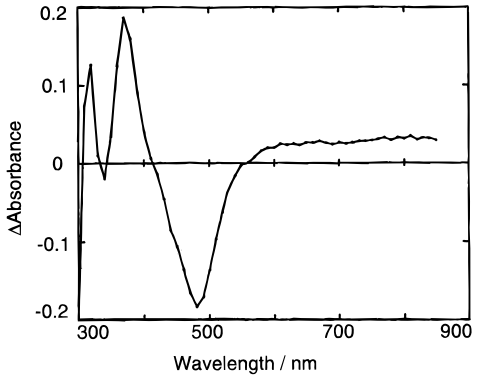

Figure 7. The TA spectra of protonated dinuclear $[(btfmb)_2Ru(bbbpyH_2)Ru(btfmb)_2]^{4+}$ (1.0×10^{-5} M with 1 mM $HClO_4$) in CH_3CN immediately after laser excitation.

Scheme 4

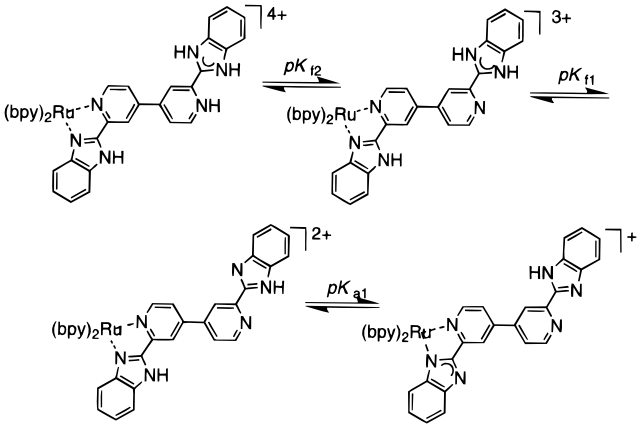

nm increases. However, only a small change of the MLCT band at 465 nm is observed. Upon further increase of pH from 5.2 to 10, the absorption maximum at 465 nm shifts to longer wavelength (472 nm), keeping the isosbestic points at 420 and 480 nm. From the analysis of the absorbance vs pH titration curve, the first pK_{f1} for protonation, probably of the free benzimidazole moiety, and the imino N−H dissociation constant, pK_{a1}, of $[Ru(bpy)_2(bbbpyH_2)]^{2+}$ are calculated as $pK_{f1} = 3.91$ and $pK_{a1} = 6.63$ (Scheme 4). Since limiting spectra could not be obtained in the more acidic pH region, an accurate second pK_{f2} for protonation of the free (2-pyridyl)benzimidazole moiety could not be determined. However, $bbbpyH_2$ becomes protonated to form the diprotonated mononuclear complex $[Ru(bpy)_2(bbbpyH_4)]^{4+}$ in 98% sulfuric acid, whereupon the complex exhibits MLCT absorption maxima at 442 and 546 nm. The reported pK_f values of coordinated 4,4′-bipyridine in Ru and Re complexes fall within a range 4−4.5.[28] Thus, the coodinated $bbbpyH_2$ ligand has a low basicity compared to unsubstituted 4,4′-bipyridine.

Dinuclear $[(bpy)_2Ru(bbbpyH_2)Ru(bpy)_2]^{4+}$ in CH_3CN−buffer (pH 2.3) exhibits a MLCT band at 499 nm. The pH dependence of the absorption spectra is shown in Figure 8. Going from pH 3.2 to 11.2, the MLCT band at 499 nm shifts to 483 nm. From regression curve fitting of plots of absorbance vs pH at 385, 485 and 523 nm (see the inset of Figure 8), the values of $pK_{a1} = 5.57$ and $pK_{a2} = 6.88$ were obtained. The pK_a value of $[(btfmb)_2Ru(bbbpyH_2)Ru(btfmb)_2]^{4+}$ became lower compared to those of bpy analogs (Table 6).

(28) (a) Lavallee, D. K.; Fleischer, E. B. *J. Am. Chem. Soc.* **1972**, *94*, 2583−2599. (b) Giordano, P. J.; Wrighton, M. S. *J. Am. Chem. Soc.* **1979**, *101*, 2888−2897.

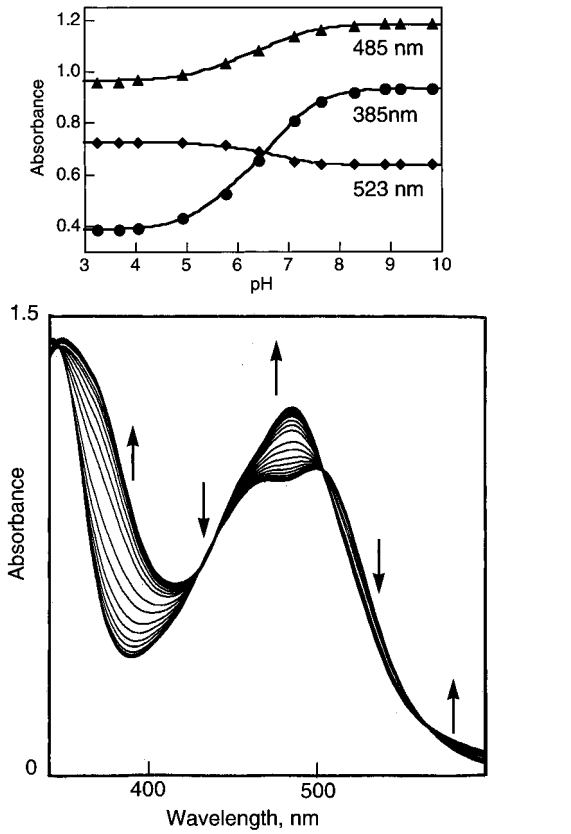

Figure 8. The pH dependence of the absorption spectra of dinuclear $[(bpy)_2Ru(bbbpyH_2)Ru(bpy)_2]^{4+}$ (3.5×10^{-5} M) in CH_3CN−buffer (1:1 v/v) at various pH values: pH = 4.36, 4.64, 4.92, 5.22, 5.52, 5.78, 6.15, 6.42, 6.88, 7.12, 7.37, 7.66, 7.95, and 8.31, and the titration curves at different wavelengths. The lines are simulated curves.

Table 6. The pK_a Values of Complexes Determined Spectrophotometrically in a CH_3CN/Buffer Solution

complex	pK_{f1}	pK_{a1}	pK_{a2}
$[Ru(bpy)_2(bbbpyH_2)]^{2+}$	3.91	6.63	
$[Ru_2(bpy)_4(bbbpyH_2)]^{4+}$		5.57	6.88
$[Ru_2(btfmb)_4(bbbpyH_2)]^{4+}$		4.87	5.81
$[Ru(bpy)_2(bpbimH_2)]^{2+}$ [a]		6.53	
$[Ru_2(bpy)_4(bpbimH_2)]^{4+}$ [a]		5.61	7.12

[a] Reference 4g.

Resonance Raman (rR) Spectra. The rR spectra of the deprotonated complexes $[(bpy)_2Ru(bbbpy)Ru(bpy)_2]^{2+}$ and $[(bpy\text{-}d_8)_2Ru(bbbpy)Ru(bpy\text{-}d_8)_2]^{2+}$ were measured with exciting laser lines in the wavelength region 546−457.9 nm, thus covering the first absorption band. In the case of the d_8-complex the emission was so strong that it prevented the recording of the rR spectra with exciting laser lines above 514.5 nm. This difference in emission between the h_8- and d_8-complexes is most likely due to the deuterium isotope effect. The spectra of $[(bpy)_2Ru(bbbpy)Ru(bpy)_2]^{2+}$ show resonance enhancement of Raman intensity for bands at 1603, 1555, and 1484 cm^{-1}, which are known to belong to symmetrical stretching modes of coordinated bpy.[2q,26] Just as for $[Ru(bpy)_3]^{2+}$, these bands are expected to shift to lower frequency upon deuteration of bpy. They are indeed observed at 1567, 1518, and 1418 cm^{-1} in the spectra of the corresponding complex $[(bpy\text{-}d_8)_2Ru(bbbpy)Ru(bpy\text{-}d_8)_2]^{2+}$ (1575, 1529, and 1427 cm^{-1} for $[Ru(bpy\text{-}d_8)_3]^{2+}$).[26] In addition, a strong band is observed at 1618 cm^{-1}. Since this band appears in the spectra of both complexes, it is assigned to a symmetric stretching vibration of the bridging ligand, bbbpy. The 1618 cm^{-1} band is the strongest Raman band upon

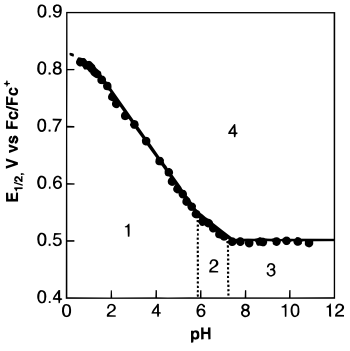

Figure 9. The half-wave potential, $E_{1/2}$, vs pH for dinuclear $[(bpy)_2Ru(bbbpyH_2)Ru(bpy)_2]^{4+}$ (1.78×10^{-4} M) in CH_3CN-buffer (1:1 v/v) at 25 °C: **1,** $[(bpy)_2Ru^{II}(bbbpyH_2)Ru^{II}(bpy)_2]^{4+}$; **2**, $[(bpy)_2Ru^{II}(bbbpyH)Ru^{II}(bpy)_2]^{3+}$; **3**, $[(bpy)_2Ru^{II}(bbbpy)Ru^{II}(bpy)_2]^{2+}$; **4**, $[(bpy)_2Ru^{III}(bbbpy)Ru^{III}(bpy)_2]^{4+}$.

excitation at the low-energy side of the first absorption band. This means that this part of the composite band belongs to the Ru → bbbpy transitions. Going to shorter wavelength excitation, the bpy bands increase in intensity at the expense of the bbbpy bands. Thus, the high-energy shoulder of the MLCT band mainly consists of the Ru → bpy transitions. In accordance with expectations, both complexes behave similarly. We may conclude from these data that the lowest π^*-orbitals of the two ligands bbbpy and bpy are very close in energy, although the orbital of bbbpy lies still somewhat lower.

Proton-Coupled Oxidation Reactions. The oxidation potentials of the mono- and dinuclear $Ru-bbbpyH_2$ complexes in CH_3CN-buffer show a strong pH dependence. From a plot of the half-wave potential $E_{1/2}$ vs pH for the mononuclear complex $[Ru(bpy)_2(bbbpyH_2)]^{2+}$ in CH_3CN-buffer (1:1 v/v), it was found that the $E_{1/2}$ values decrease linearly with a slope of −60 mV at $1.5 < pH < 6.9$. This is consistent with a reversible one-proton, one-electron process (eq 1).

$$[Ru^{II}(bpy)_2(bbbpyH_2)]^{2+} \rightarrow [Ru^{III}(bpy)_2(bbbpyH)]^{2+} + H^+ + e^- \quad (1)$$

At $pH > 6.9$, the slope of $E_{1/2}$ vs pH is independent of pH and the process can be represented as

$$[Ru^{II}(bpy)_2(bbbpyH)]^{+} \rightarrow [Ru^{III}(bpy)_2(bbbpyH)]^{2+} + e^- \quad (2)$$

The breakpoint of these two lines gives $pK_a = 6.9$, which is consistent with the value obtained by the spectrophotometric method.

Similarly, the cyclic voltammogram of the dinuclear complex exhibits only one two-electron oxidation wave over the whole pH range. Even changing the solution pH did not lead to any difference in peak separation for the dinuclear $bbbpyH_2$ complex. This suggests that the difference between the first and the second oxidation potentials in two successive one-electron processes has not changed. This observation is in contrast with the electrochemical behavior of the $bpbimH_2$ complex.[4b]

Figure 9 shows the half-wave potential, $E_{1/2}$, vs pH diagram for the dinuclear complex $[Ru(bpy)_2(bbbpyH_2)Ru(bpy)_2]^{4+}$, where the half-wave potential, $E_{1/2}$, is calculated as the average of the anodic and cathodic peak potentials. Over the pH range 1.6−5.6, the $E_{1/2}$ value decreases linearly with increasing pH with a slope −60 mV/pH unit, indicative of a two-electron, two-proton step (eq 3).

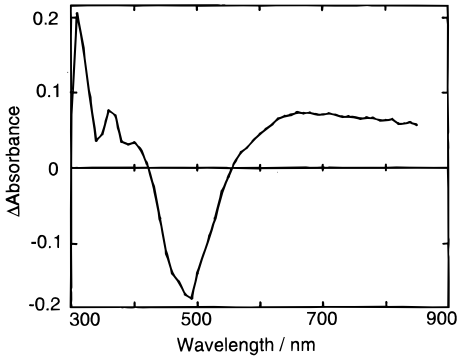

Figure 10. The TA spectra of deprotonated dinuclear $[(bpy)_2Ru(bbbpy)Ru(bpy)_2]^{2+}$ (1.0×10^{-5} M) in CH_3CN immediately after laser excitation.

$$[(bpy)_2Ru^{II}(bbbpyH_2)Ru^{II}(bpy)_2]^{4+} \rightarrow [(bpy)_2Ru^{III}(bbbpy)Ru^{III}(bpy)_2]^{4+} + 2H^+ + 2e^- \quad (3)$$

At $5.6 < pH < 7.2$, the slope of $E_{1/2}$ vs pH was −30 mV/pH, which is consistent with the two-electron, one-proton reaction as shown in eq 4.

$$[(bpy)_2Ru^{II}(bbbpyH)Ru^{II}(bpy)_2]^{3+} \rightarrow [(bpy)_2Ru^{III}(bbbpy)Ru^{III}(bpy)_2]^{4+} + H^+ + 2e^- \quad (4)$$

Above pH 7.2, the Ru(II/III) couple is independent of the pH (eq 5).

$$[(bpy)_2Ru^{II}(bbbpy)Ru^{II}(bpy)_2]^{2+} \rightarrow [(bpy)_2Ru^{III}(bbbpy)Ru^{III}(bpy)_2]^{4+} + 2e^- \quad (5)$$

pK_a values of 5.6 and 7.2 were obtained as breakpoints and are consistent with those obtained from spectrophotometric measurements.

Transient Absorption Spectra. Figure 10 shows the TA spectrum of the isolated deprotonated dinuclear complex in CH_3CN, with a bleaching at 490 nm and absorption enhancement at 310, 360, and 675 nm. The TA at these wavelengths decayed with the same rate (20 ns) as the phosphorescence monitored at 715 nm. This means that the TA spectrum represents the formation of the lowest excited CT state.

In contrast to the TA spectrum of the protonated dinuclear complex (Figure 6b), the band around 360 nm is relatively weak compared to the band at 310 nm. Furthermore, no bleaching of the $\pi-\pi^*$ transition of bbbpy at 344 nm is observed, and the strong band of bpy^- at 370 nm does not show up. Comparing this result with the reported TA spectra of $[Ru(bpy)_3]^{2+}$ and other relevant Ru−bpy complexes,[4c−e] the band around 360 nm arises from the fact that the bands of bpy^- and/or $bbbpy^-$ cancel out the bleaching of the strong $\pi-\pi^*$ transition of bbbpy around 350 nm. The weak band in the ∼650 nm region also indicates a transition of $bbbpy^-$ in addition to the $\pi-\pi^*$ transitions of both bpy^- and bpy coordinated to Ru(III). Consequently, this TA spectral feature indicates that the excited electron is localized on both the peripheral bpy ligand and bbbpy. Thus, the lowest excited states of the dinuclear complexes can be summarized in Scheme 5.

Deprotonation Effect on the IT Band. Flow oxidative electrolysis of $[(bpy)_2Ru(bbbpyH_2)Ru(bpy)_2]^{4+}$ in CH_3CN gave the characteristic near-infrared spectrum of a mixed-valence Ru(II)−Ru(III) complex. When the applied potential was made more positive, a new band at 1200 nm (8330 cm^{-1}) first increased and then decreased in intensity, whereas the band at

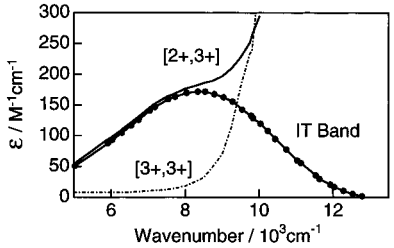

Figure 11. The calculated intervalence charge-transfer (IT) band of $[(bpy)_2Ru(bbbpyH_2)Ru(bpy)_2]^{4+}$ in CH_3CN (with 10 mM $HClO_4$) by the flow-through electrolytic method. The spectra were corrected by considering the comproportionation equilibrium, $K = 4.1$.

Scheme 5

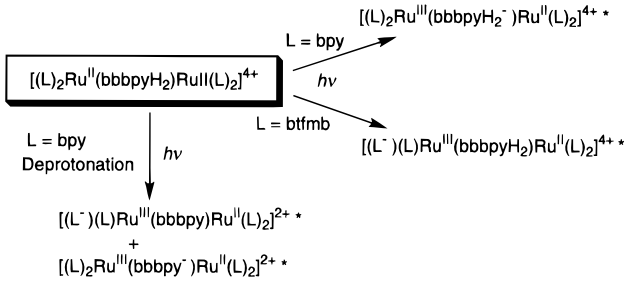

680 nm only increased in intensity. On the basis of this observation, the bands at 1200 and 680 nm are assigned to an intervalence charge transfer (IT) and a ligand-to-metal charge transfer (LMCT) transition, respectively. The anodic current, i, can be written as

$$n = \frac{i}{vF[\mathrm{M}]_0}$$

where n = the number of electrons oxidized in the flow electrolysis, v = flow rate, i = anodic current, F = Faraday constant, and $[M]_0$ = initial concentration of the complex. From analysis of the plot of absorbance vs current, the comproportionation constant can be determined as $K_{com} = 4.1$. By using this comproportionation constant, the IT band can be calculated as shown in Figure 11.

From this spectrum, the absorbance maximum of the IT transition was found to be at 1200 nm, with an extinction coefficient of 170 M^{-1} cm^{-1}. On the other hand, no IT band below 1000 nm was observed for $[(btfmb)_2Ru(bbbpyH_2)Ru(btfmb)_2]^{4+}$ in CH_3CN.

The degree of electronic coupling between the metal centers, H_{AB}, can be evaluated from the position, bandwidth, and intensity of the IT band through the following equation:[29]

$$H_{AB} = 2.05 \times 10^{-2} \left[\frac{\epsilon_{max}\Delta\nu 1/2}{\nu_{max}}\right]^{1/2} \left[\frac{\nu_{max}}{r}\right] (\text{in cm}^{-1})$$

where ϵ_{max} is the extinction coefficient (in M^{-1} cm^{-1}), ν_{max} is the wavenumber of the IT absorption maximum (in cm^{-1}), $\Delta\nu_{1/2}$ is the bandwidth at half-height (in cm^{-1}), and r is the distance between the metal sites (in Å). For the present $bbbpyH_2$-bridged system, a value $r = 11$ Å was estimated from molecular models. The calculated H_{AB} value is 120 cm^{-1}, which is relatively small compared with those reported for systems of other bridging ligands such as $bpbimH_2$. When the bridging $bbbpyH_2$ ligand was deprotonated, the IT band could unfortunately not be observed. This may be due to a smaller metal−metal interaction in the deprotonated form compared to that in the protonated form or to overlap with the strong LMCT band at 780 nm. The latter explanation is not very probable, since the intervalence band for dinuclear complexes containing the benzimidazole and benzimidazolate have been separated from the LMCT band.[4]

Scheme 6. The Effect of Deprotonation on Orbital Interactions in the Mixed-Valence Dinuclear Ru Complex

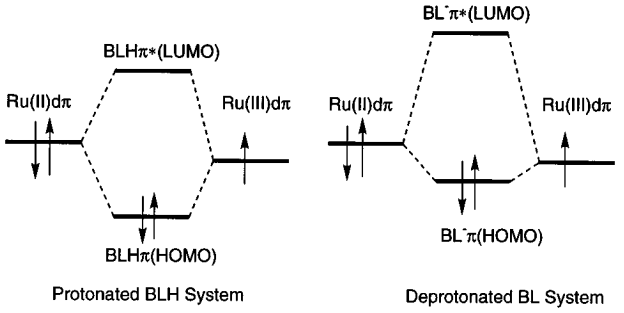

The strength of electronic coupling between two Ru ions depends on orbital mixing between the Ru(II) or Ru(III) ion and the HOMO/LUMO orbitals of the bridging ligand as shown in Scheme 6, where BLH stands for the protonated state of the bridging ligand and BL^- for the deprotonated one. Molecular orbital calculations of $bbbpyH_2$ and its deprotonated form indicate that the 4,4′-bipyridine moiety does not take part in the HOMO but does in the LUMO. Since the 4,4′-bipyridine moiety can be considered to act as a superexchange pathway, the metal−metal interaction is governed by the electron density in this LUMO π^*-orbital. The high electron density on the 4,4′-bpy moiety of the LUMO ($bbbpyH_2$) suggests that a Ru(II)dπ−$bbbpyH_2$ π^* (ligand LUMO) interaction exists. On the other hand, deprotonation of the bridging $bbbpyH_2$ moiety induces an increase of orbital energies, and the orbital interaction between Ru(II)dπ and the bridging bbbpy π^*-orbitals will decrease. Similarly, lowering of the Ru dπ orbitals by use of btfmb as peripheral ligands also decreases the interaction between Ru dπ and the bridging bbbpy π^*-orbitals, which leads to the lack of an observable IT band in $[(btfmb)_2Ru(bbbpyH_2)Ru(btfmb)_2]^{4+}$. This is in sharp contrast to the $bpbimH_2$ system, in which the Ru(III)dπ−ligand π HOMO interaction increased when the bridging $bpbimH_2$ ligand was deprotonated. In conclusion, deprotonation of the bridging ligand increases the metal−metal interaction when the Ru(III)dπ−BL^- π interaction is predominant. On the other hand, deprotonation decreases the interaction when the Ru(II)dπ−BL^- π^* interaction is predominant.

Conclusion

The new bridging ligand 2,2′-bis(benzimidazol-2-yl)-4,4′-bipyridine (4,4′-$bbbpyH_2$) has a relatively strong π-acceptor property because of the presence of low-energy π^*-orbitals. In this way it is distinct from the isomeric 2,2′-bis(2-pyridyl)-bibenzimidazole ($bpbimH_2$) bridging system. 4,4′-$BbbpyH_2$ can form mono- and dinuclear Ru−bipyridine complexes. Since deprotonation increases the bridging ligand π/π^*-orbital energies, the orbital mixing between the Ru dπ and bridging ligand π/π^*-orbitals is changed; i.e., hole-type superexchange through the bridging ligand π-orbital to the Ru(III) dπ charge-transfer state is favored upon deprotonation, whereas electron-type superexchange through the Ru(II) dπ to the bridging ligand π^*-orbital charge-transfer state is disfavored. Deprotonation of the 4,4′-$bbbpyH_2$ bridging ligand decreases the metal-metal interaction as a result of smaller orbital mixing between the Ru(II)dπ and bridging ligand π^*-orbitals. Similar proton-induced tuning

(29) Creutz, C. *Prog. Inorg. Chem.* **1983**, *30*, 1.

of the chemical properties has been reported for the dipyridyltriazole system.[30] Concerning the metal-metal interaction in the 4,4′-bbbpyH_2- and bpbimH_2-bridged dinuclear complexes, it was shown that the intervening fragment (i.e., bibenzimidazole vs 4,4′-bipyridine) in the bridging ligand plays an important role.

Acknowledgment. M.H. gratefully acknowledges financial support from the Ministry of Education for a Grant-in-Aid for Scientific Research (No.04453045 and 06804036), the Sumitomo Foundation for a basic science grant, and the Japan Securities Scholarship Foundation. M.H. also thanks Ishihara Sangyo Kaisha, Ltd., for their gift of trifluoromethyl-substituted chloropyridine and Dr. M. Furue at Osaka University for his kind advice on the synthesis of the btfmb ligand. M.M.A. also thanks the Ministry of Education for a Japanese Government (Monbusho) Scholarship. The work was supported, in part, by the Joint Studies Program (1992−1993) of the Institute for Molecular Science, Okazaki, Japan, with Prof. K. Nakasuji. We thank Th. L. Snoeck for measuring the Raman spectra.

Supporting Information Available: Tables giving anisotropic thermal parameters (Table S1) and complete tables of bond distances and angles (Table S2) and ORTEP drawings of the crystal structures (Figure S1) (7 pages). Ordering information is given on any current masthead page.

IC950083Y

(30) (a) Nieuwenhuis, H. A.; Haasnot, J. G.; Hage, R.; Reedijk, J.; Snoeck, T. L.; Stufkens, D. J.; Vos, J. G. *Inorg. Chem.* **1991**, *30*, 48−54. (b) Hage, R.; Haasnoot, J. G.; Reedijk, J.; Wang, R.; Vos, J. G. *Inorg. Chem.* **1991**, *30*, 3263−3269.